CHALMERS

Modeling and Energy Consumption Determination of an Electric Go-kart

Master of Science Thesis in the Programme Electric Power Engineering

DIDI ISTARDI

Department of Energy and Environment
Division of Electric Power Engineering
CHALMERS UNIVERSITY OF TECHNOLOGY
Göteborg, Sweden, 2009

Modeling and Energy Consumption Determination of an Electric Go-kart

DIDI ISTARDI,

Supervisor: Anders Lindskog

Examiner: Prof. Torbjörn Thiringer

Department of Energy and Environment
Division of Electric Power Engineering
Chalmers University of Technology
SE-412 96 Göteborg
Sweden

Telephone + 46 (0)31-772 1000

Department of Energy and Environment

Göteborg, Sweden 2009

ACKNOWLEDGEMENT

I am especially grateful to my examiner Prof. Torbjörn Thiringer and my supervisor Anders Lindskog for their help, support, and guidance during this master thesis work. Thank you so much for your dedication and patience.

Thank you so much to the Ministry of Communication and Information Technology, Republic of Indonesia, and Batam Polytechnics for financial support during my study at Chalmers University of Technology, Sweden.

I also want to thank Stig Ekstrom from the *Svenska Bilsportförbundet (Sekreterare i Kartingutskottet)* for his discussion inputs and the opportunity he gave us in this thesis work.

Many thanks to Abba, Ragnar, Pema, and others for their discussion, input, and wonderful time we spent together at the master thesis room.

I also want to thank the Indonesian community at Göteborg, who has been my second family here in Sweden, and my Indonesian fellow students in Göteborg (Olof, Volrat) for their kindness and friendship. Special thanks to Setyo and Risma for their corrections in my report.

I also would like to thank all of the EPE master students 2007, the bachelor students that carry on the electric go-kart project for their kind help, and also thanks to Magnus, Robert, and Aleksander.

Finally, my thanks come to my family in Indonesia for their support.

ABSTRACT

An electric traction motor drive for an electric karting application was modeled for efficiency studies and simulated using the Matlab®/Simulink® software. In this thesis, the electric traction motor drive model includes models of battery, power electronic converter, and electric motor losses related to a typical 48 seconds track driving schedule. The important losses within a typical electric motor such as stator copper, rotor copper, and core losses were modeled and simulated over the entire speed range. A power electronic converter was modeled; including the switching and conduction losses for both MOSFETs and the anti parallel power diodes. The energy storage was modeled as a generic model capable of representing losses and the state of charge (SOC) of the battery over the driving cycles. The energy captured during regenerative braking was also considered in the simulation. Finally, the overall electric traction motor drive system efficiency was estimated based on the individual model based efficiency analysis. The battery and induction motor parameters, which were used in the simulation, were calculated using the measurement data obtained through laboratory tests.

The complete electric traction drive system was simulated and observed using the drive cycle of the ICE karting at the race day for 48 seconds (one lap). The total average efficiency of the electric drive system is 66.7%. The average power of the electric motor was 5.4 kW and the total energy consumed by this electric traction drive system was 920 Wh for one whole race. The battery can supply the electric traction drive system for 22 minutes. The regenerative braking energy can be used to charge the battery and reduce the energy usage in the system, but has only a small effect due to the short time of the regenerative braking period.

Keywords: Loss modeling, induction motor, electric karting, regenerative braking, battery.

Table of Contents

List of Symbols and Subscripts

Symbols

a	gear ratio/coupling ratio
A	frontal surface area of vehicle [m^2]
B	damping [kgm^2/s]
c	a constant that takes into account the bar material and shape
C	coefficient at vehicles dynamics model
d	bar depth [m]
D	duty cycle
e	electromotive force voltage [V]
E	battery voltage [V]
f	frequency [Hz]
F	force [Nm]
g	gravitational acceleration [m/s^2]
I	current [A]
J	moment inertias [kgm^2]
k	coefficient given by material and design of motor
L	inductances [H]
m	total vehicle mass [kg]
M	modulation index
n	number of teeth the gear
N	ratio between switching and fundamental frequency
p	number of poles in electric motor
P	the motive power [W]
Q	capacity of battery [Ah]
r	radius of wheel [m]
R	resistance [Ω]
s	slip of induction motor
S	snappiness factor for the diode
T	torque at wheel [Nm]
v	speed [m/s^2]
v_a	relative vehicle speed with respect to the air [m/s]
V	voltages [V]
W	energy [Wh]
Z	impedance
δ	specific air density [kg/m^3]
ω	angular speed [rad/sec]
ϴ	angle position [rad]
ø	flux density [Wb]
α	temperature coefficient
τ	carrier period [s]

Subscripts

a	achieved value
ac	alternating
ad	aerodynamic drag
af	acceleration force
ave	average values
c	collector

cr	climbing resistance
cu	copper
cond	conduction
CE	collector – emitter
d	developed at electric motor rotor
dc	Direct
D	diode
e	eddy current
fe	Iron
g	air gap
h	hysteresis
L	Load
m	magnetizing part in electric motor
mech	mechanical (windage and friction)
n	harmonics
o	open circuit
on	on state
off	off state
Q	power switching device
r	electric motor rotor
rr	rolling resistance
rms	root mean square values
R	reverse recovery
s	electric motor stator
sc	locked rotor
sw	switching
str	Stray
t	Wheel
T_1	temperature T_1
T_2	temperature T_2

1. INTRODUCTION

The first electric vehicle was made in the 1830s and was popular for almost a century [1][2][3]. However, since 1933 the number of electric vehicles have decreased due to the improvements of the internal combustion engine (ICE) that has become better and cheaper. Nowadays, environmental considerations, energy costs, and improvements in control and battery technology have inspired an increasing amount of research and development of electric vehicles.

One of the developments in the electric vehicle is research on electric kart racing or karting. Electric karting is a variant of an open-wheel motor sport, with small four-wheeled vehicles called karts. These karts are simple and usually raced on a scaled-down track. Since the electric kart engine is powered by an electric motor instead of an internal combustion engine and the motor is operated using the power stored in batteries [4], its engine has many advantages over the ICE. It is pollution-free, has higher energy conversion efficiency and less vibration, requires low maintenance, its speed is easy to control and it can use the energy from regenerative braking [1],[3]. An electric karting race was first started in 1989 in Italy [5] and is currently getting popular in the United States and Europe due to improvements in control and battery technology.

The components of electric karting are chassis made of a steel tube, a propulsion system that includes an electric motor that drives the wheels, a power electronic converter that regulates the energy flow to the motor and a transmission system, a battery that provides energy, and a control unit that ensures a proper operation of the power electronic converter [3],[6],[7].

1.1. Objective of the Thesis

The purpose of this thesis is mainly to show the possibilities of creating a zero-pollution alternative that is suitable in karting. In order to observe and analyze the energy use in the karting, modeling and simulation of an electric traction motor drive with an efficiency model were done using Matlab®/Simulink® software. The electric traction motor drive model includes the models of battery, power electronic converter, and electric motor losses.

The proposed electric traction motor drive system for the electric karting should fulfill the following requirements specified by the *Svenska Bilsportförbundet* (the Swedish Automobile Sports Federation):

- the system shall give zero pollution.
- the engine shall be optimized for 10 minutes heat in full race and 3 minutes for in and out laps.
- the recharging of batteries shall be less than 30 minutes to get enough energy for the next heat.
- the batteries shall maintain enough capacity after a minimum of 1000 discharge/recharge cycles.
- the total drive package system weight must be less than 25 kg.
- this drive shall be able to start without any assistance while the driver is seated.

1.2. Thesis Outline

The report of this thesis is arranged in seven chapters. The first chapter consists of an introduction of the project, presenting the aim and scope of the thesis and steps performed to accomplish the aim.

Chapter Two includes the theoretical background of the electric traction motor drive system, such as transmissions or dynamic behaviors of the vehicle model, the electric motor model using a loss model, power electronic converter and controller loss model, as well as battery model. This chapter also describes the basic theory of regenerative braking.

Chapter Three presents the case setting of the problem and the known parameters used as simulation input and explains the basic criteria to select the drive system components in electric karting.

Chapter Four presents the measurement of battery parameters and induction motor parameters in laboratory and the performance analysis of the measurement.

Chapter Five presents modeling blocks of the electric karting drive system and battery using MATLAB®/Simulink®, and discusses several characteristics of the electric traction drive system and battery.

Chapter Six presents the evaluation of the complete electric traction drive systems and the safety in electric karting.

Finally in Chapter Seven, the overall conclusions of the thesis work are given and the recommendations for future work are given.

2. BASIC MODELING OF ELECTRIC TRACTION DRIVE SYSTEM

In this chapter, theory about electric traction drive system will be explained. A simple electric traction drive system consists of a drive system (transmission, electric motor, and power electronics) and an energy storage (battery) [6] as seen in Figure 2.1. Examples of some papers that describe the modeling of an electric traction drive system using MATLAB® or other software [7]-[10].

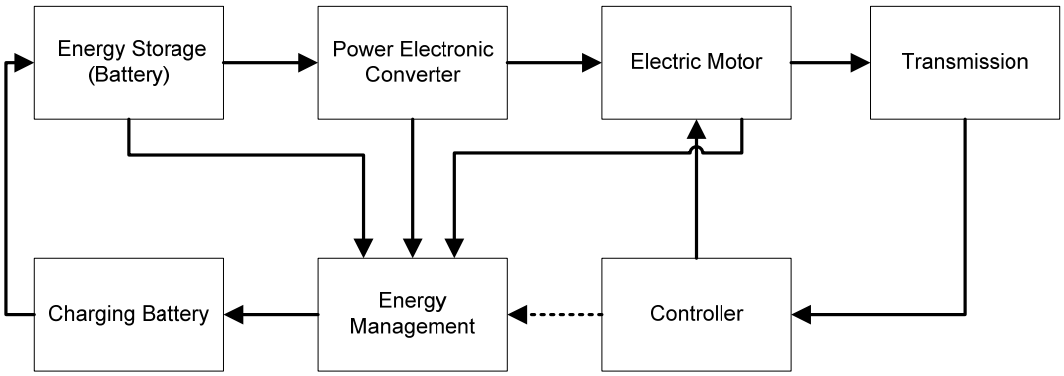

Figure 2.1 Block diagram of drive system for electric karting

Within the system, energy is stored in the battery. A power electronic converter connects the battery to an electric motor. The voltage and current output of the battery are maintained to match the ratings of the electric motor. The electric motor converts electrical energy supplied by the battery into mechanical energy. A transmission transforms the mechanical energy into a linear motion. Speed and torque are adjusted using the gear box. The gear can transmit the rotational force at different speeds, torque, and directions. A controller and energy management control the speed and direction of the electric karting, and optimize the energy conversion from the battery to the transmission. The battery can be charged from the line power and also from regenerative braking.

2.1. Model of Transmission (Vehicle Dynamic Model)

Mechanical energy provided by the electric traction drive system is used to drive the wheels of the electric karting. The supplied energy must be large enough to overcome the "traction resistance", i.e. the sum of rolling resistance, aerodynamic drag, climbing resistance and acceleration force [8], [11]. Rolling resistance is a deformation process mechanism which occurs at the contact patch between the tires and road surface. Aerodynamic drag is the viscous resistance of air upon the vehicle. In this thesis, the race track is assumed to be flat, thus the climbing resistance is neglected. Those forces can be calculated using:

$$F_t = F_{ad} + F_{rr} + F_{cr} + F_{af} \tag{2.1}$$

$$F_{ad} = \frac{1}{2}\delta C_{ad} A v_a^2 \tag{2.2}$$

$$F_{rr} = C_{rr} mg \tag{2.3}$$

$$F_{af} = ma\ . \tag{2.4}$$

The motive power required to run the vehicle is calculated as:

$$P_t = F_t v_t\ . \tag{2.5}$$

The engine torque at the wheel is obtained using:

$$T_t = F_t r \,. \tag{2.6}$$

In this thesis, the moment of inertia has to be taken into consideration.
Air density for this simulation is set at 1.225 kg/m^3.

The relation between the two sides of the gear can be formulated using:

$$\frac{T_r}{T_t} = \frac{\omega_t}{\omega_r} = \frac{\theta_t}{\theta_r} = \frac{n_r}{n_t} = a. \tag{2.7}$$

Calculation of the torque generated by the electric motor is based on energy considerations in terms of inertias, load acceleration, coupling ratio, and the load torque or force as shown below:

$$T_r = J\frac{d\omega_r}{dt} + B\omega_r + T_L \,. \tag{2.8}$$

2.2. Modeling of Electric Motor Losses

In order to calculate the efficiency of the electric karting, it is essential to understand how the losses of each component change with speed. The losses in the electric motor can be divided into 4 components [12]: copper losses, core losses, mechanical losses and stray losses.

Copper losses (stator and rotor losses) are the I^2R heat losses resulting from current flow in the windings. The copper losses are variable, depending on the current and hence the load on the machine. The copper losses measurement requires the consideration of temperature and skin effect in the winding resistance.

Core losses (iron losses) are losses which occur in the magnetic circuit. Normally these losses comprise of hysteresis loss and eddy current loss. Hysteresis loss is the energy needed to magnetize and demagnetize the iron in the magnetic circuit during each voltage period. It depends on the flux and the frequency. Eddy current loss occurs due to the unwanted circulating currents induced in the iron of the magnetic circuit by the windings. The most common way of modeling core losses is to use the following Steinmetz expression of these losses [13]:

$$P_e = k_e \emptyset^2 f^2 \tag{2.9}$$

$$P_h = k_h \emptyset^{1.6} f \,. \tag{2.10}$$

In an electric motor, there are two iron cores (except in permanent magnet rotor): stator core ($P_{fe,s}$) and rotor core ($P_{fe,r}$). The frequency in rotor core depends on rotor speed. The total core losses can be calculated as:

$$\begin{aligned} P_{fe} &= P_{fe,s} + P_{fe,r} \\ &= [k_e \emptyset^2 f_s^2 + k_h \emptyset^{1.6} f_s] + [k_e \emptyset^2 f_r^2 + k_h \emptyset^{1.6} f_r] \,. \end{aligned} \tag{2.11}$$

Mechanical losses are losses resulting from the drag on the rotor movement. These losses include friction and windage losses. These losses are a function of motor speed and do not depend on the type of power supply, as seen in [12].

$$P_{mech} = k_{mech} \omega_r^3 \tag{2.12}$$

Stray losses represent group of losses that are not covered in the previous categories. These losses can be modeled as in [12].

$$P_{str} = k_{str}\left[\frac{k_h}{f_n} + k_e\right]V_{str}^2 \tag{2.13}$$

The stator and rotor winding resistances increase with temperature. The temperature increase can be calculated and an approximated correction factor can be used to find the correct stator and rotor winding resistances. Both resistances can be corrected from temperature effect by using [12].

$$R_{T2} = R_{T1}\big(1 + \alpha_{cu}(T_2 - T_1)\big) \tag{2.14}$$

The skin effect on winding resistance can be calculated using

$$R_{ac} = R_{dc}(1 + cdf_n^{0.5})\,. \tag{2.15}$$

In this thesis, only copper and iron losses will be used in simulation and analysis. Mechanical and stray losses are disregarded.

2.2.1. Modeling of Induction Motor Losses

Induction motor with squirrel cage rotor is widely used in industry due to its simplicity, minimum maintenance requirement, and low costs [14]-[16]. The induction motor is composed of a stator circuit and a rotor circuit. In the three-phase induction motor, the stator circuit has three sets of coils that are separated by 120^0 and excited by a three-phase supply. The rotor circuit is also designed with three-phase windings that are shorted internally or externally (through slip rings and brushes) [16]-[18]. The per-phase equivalent circuit of the induction motor at steady state is shown in Figure 2.2.

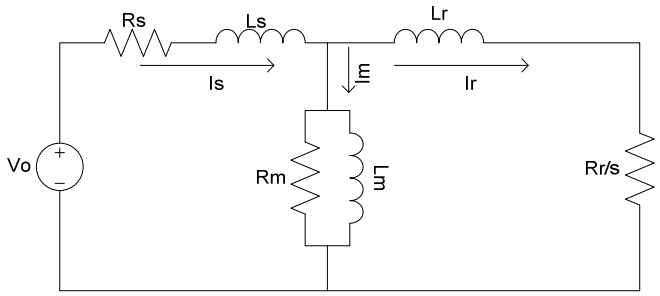

Figure 2.2 Equivalent circuit of induction motor

In the rotor circuit, the rotor resistance $\frac{R_r}{s}$ consists of two components: the losses of the rotor windings and the developed power or the load of motor. This developed power includes the mechanical and rotational loads (the friction and windage loads). Hence, the resistance $\frac{R_2}{s}$ can be rewritten as in [15]:

$$\frac{R_r}{s} = R_r + \frac{R_r}{s}(1 - s). \tag{2.16}$$

The mechanical synchronous speed (ω_{sm}) of the induction motor with p poles and supplied by the frequency f can be found using [20]

$$\omega_{sm} = \frac{2}{p}(2\pi f) = \frac{2}{p}\omega_s. \tag{2.17}$$

The power flow of the induction motor is shown in Figure 2.3. Double-lined rectangles indicate the power forms analyzed in this thesis. The rotational (mechanical) losses are neglected, thus the output power of the electric motor equals the developed power.

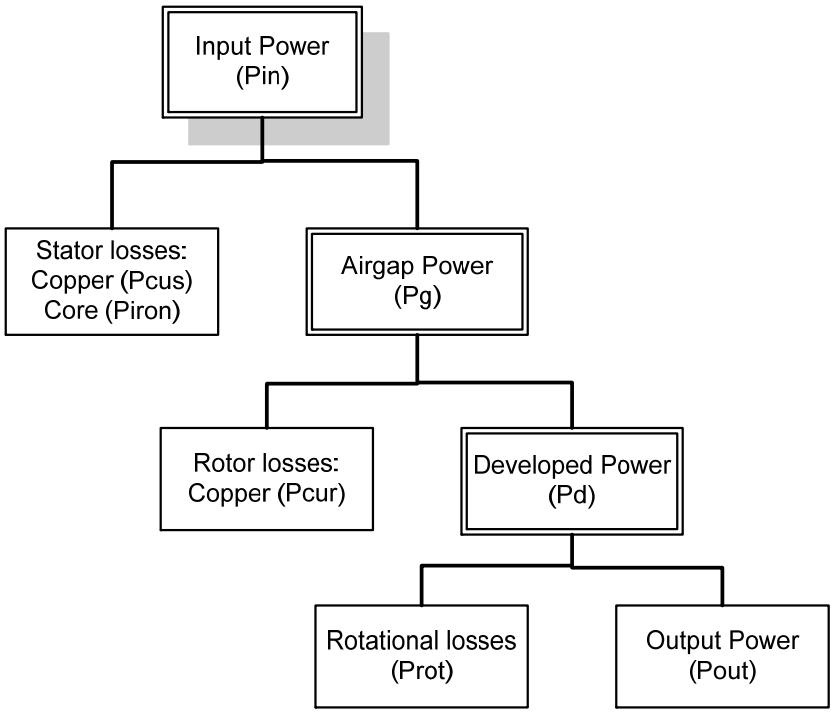

Figure 2.3 Power flow of induction motor

The power flow in the induction motor is calculated using [14]-[15]

$$P_g = 3I_r^2 \frac{R_r}{s} = T_d \omega_{sm} \tag{2.18}$$

$$P_d = 3I_r^2 \frac{R_r}{s}(1-s) = (1-s)P_g = T_d \omega_r. \tag{2.19}$$

From (2.17) and (2.18), the rotor current is expressed by

$$I_r = \sqrt{\frac{2T_d \omega_s s}{3pR_r}}. \tag{2.20}$$

Using the current divider laws, the stator current is calculated by

$$I_s = \frac{Z_m + Z_r}{Z_m} I_r \tag{2.21}$$

where Z_m and Z_r can be expressed by

$$Z_m = \frac{j\omega_s L_m R_m}{j\omega_s L_m + R_m} \tag{2.22}$$

$$Z_r = \frac{R_r}{s} + j\omega_s L_r \,. \tag{2.23}$$

From (2.21) – (2.23), the stator current will be:

$$I_s = \frac{\frac{j\omega_s L_m R_m}{j\omega_s L_m + R_m} + \frac{R_r}{s} + j\omega_s L_r}{\frac{j\omega_s L_m R_m}{j\omega_s L_m + R_m}} I_r$$

$$= \frac{\left[\frac{j\omega_s L_m R_m}{j\omega_s L_m + R_m} + \frac{R_r}{s} + j\omega_s L_r\right] j\omega_s L_m + R_m}{j\omega_s L_m R_m} I_r$$

$$I_s = \frac{\left(\frac{R_m R_r}{s} - \omega_s^2 L_r L_m\right) + j\left[\omega_s\left(R_m L_m + \frac{R_r}{s} L_m + R_m L_r\right)\right]}{j\omega_s L_m R_m} I_r$$

$$I_s = \frac{\sqrt{\left(\frac{R_m R_r}{s} - \omega_s^2 L_r L_m\right)^2 + \left[\omega_s\left(R_m L_m + \frac{R_r}{s} L_m + R_m L_r\right)\right]^2}}{\omega_s L_m R_m} I_r \,. \tag{2.24}$$

From (2.20) and (2.23), the air gaps voltage can be calculated by

$$V_g = Z_r I_r = \sqrt{\frac{s\omega_s T_d}{3R_r}\left(\frac{R_r^2}{s^2} + \omega_s L_r^2\right)}. \tag{2.25}$$

The total rated losses of the induction motor can be obtained as

$$P_{losses} = 3\left[R_s I_s^2 + R_r I_r^2 + \frac{V_g^2}{R_m}\right]. \tag{2.26}$$

These total rated losses are used to calculate both the core and copper losses at various speeds and torque levels along the drive cycle.

The induction motor can operate above the rated speed by using frequency or voltage control variations because of its rugged mechanical construction [10], [19]-[22]. The torque and power capabilities as a function of rotor speed can be seen in Figure 2.4. In the below rated speed area, the flux in the air gap is kept constant by controlling V_s/f and the value of the slip is small. Then the electric motor can produce torque until up to its rated torque and as a result, the rotor current may be assumed to be proportional to the developed torque. Therefore, this region is called "constant torque region". Based on these assumptions, the copper losses can be expressed by

$$P_{cu\_a} = \left[\frac{P_a}{\omega_a}\frac{\omega_{rated}}{P_{max}}\right]^2 P_{cu} = \left[\frac{P_a}{\omega_a}\frac{\omega_{rated}}{P_{max}}\right]^2 [3R_s I_s^2 + 3R_r I_r^2] \tag{2.27}$$

The eddy current loss component of the core loss is proportional to the square of the flux and the frequency [20] as described in (2.9). In the constant torque region, the flux is assumed constant, thus the eddy current loss is proportional to the square of the frequency only. The hysteresis loss component is proportional to the flux to the power of 1.6 and to the frequency as described in (2.10). Therefore, the total core loss in the constant torque region can be calculated by

$$P_{fe\_a} = \left[\frac{\omega_a}{\omega_{rated}}\right]^2 P_e + \left[\frac{\omega_a}{\omega_{rated}}\right] P_h \,. \tag{2.28}$$

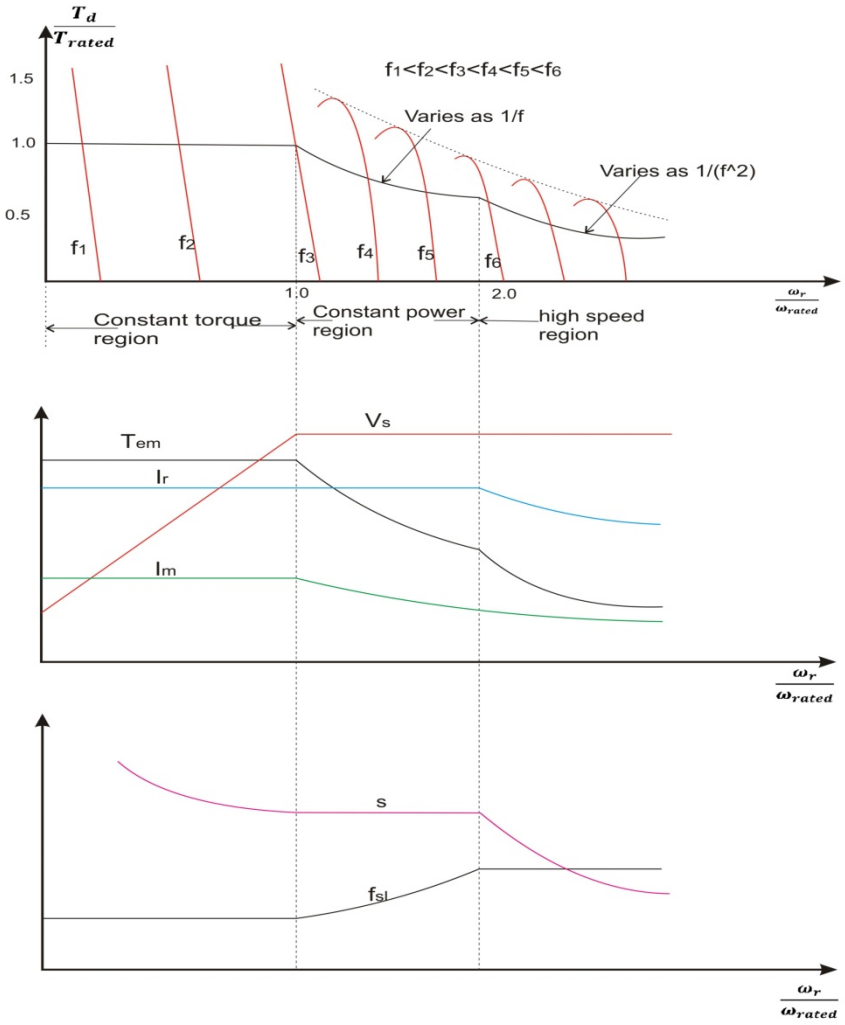

Figure 2.4 Induction motor characteristic and capabilities

To increase the motor speed above the rated speed, the stator voltage is kept at the rated voltage and the stator frequency is increased to a value above the rated frequency. So, the V_s/f is reduced and the flux is also reduced by the ratio of the instantaneous operating speed to the rated speed. At these assumptions, the developed power will remain constant and the copper losses become

$$P_{cu\_a} = \left[\frac{P_a}{P_{max}}\right]^2 [3R_s I_s^2 + 3R_r I_r^2]\,. \tag{2.29}$$

At above the rated speed, the flux in the core varies inversely with respect to frequency. So, the product of the flux and frequency is constant. With these assumptions, the eddy current losses at this region can be assumed to be constant at the rated value and the hysteresis losses are still proportional to the power of 1.6 of the frequency.

$$P_{fe\_a} = P_e + \left[\frac{\omega_a}{\omega_{rated}}\right]^{1.6} P_h \tag{2.30}$$

Even higher speed can be achieved by reducing the air gap flux until the motor torque reaches its pull-out torque. As shown in Figure 2.4, the torque and rotor current decrease with speed. As a result, the rotor losses also decrease.

The efficiency of the induction motor can be calculated by

$$\mu_{motor} = \frac{T_d \omega_r}{T_d \omega_r + P_{fe} + P_{cu}} \, x \, 100\% \, . \tag{2.31}$$

2.3. Modeling of Power Electronic Converter Losses

The power electronic converter used in this simulation is a standard six-switch three-phase bridge inverter. The aim of this component is to provide appropriate mean values of parameters commonly used in electric motor. The power electronic component as power switching device used in this thesis is MOSFETs (*Metal Oxide Semiconductor Field Effect transistors*) or IGBTs (*Insulated Gate Bipolar Transistors)* and anti-parallel power diodes. The controller pulse used in this simulation is a three-phase *pulse-width modulation* (PWM). The main losses in the converter are the conduction losses (P_{cond}) and switching losses (P_{sw}) for each switching component [10],[20].

The switching process and conduction process of the power electronics components can be seen in Figure 2.5.

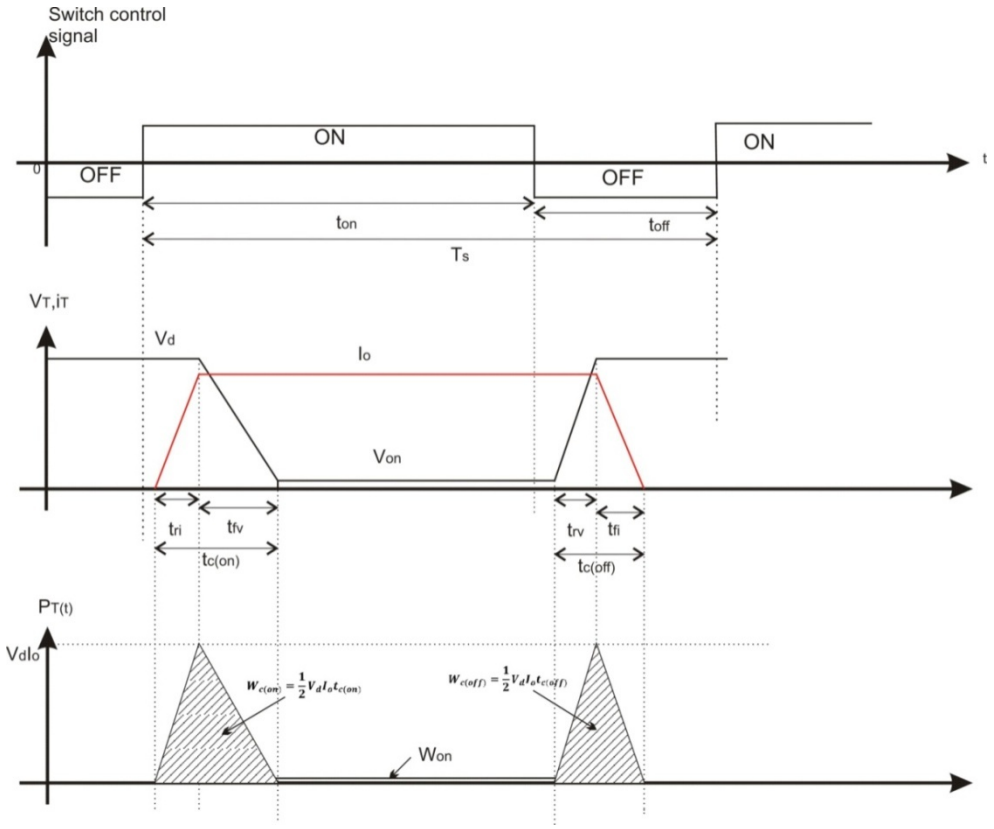

Figure 2.5 Generic-switch switching characteristics (linearized): switching wave form and instantaneous switch power loss

This switching process depends on the load and switching strategies [20],[22]. Figure 2.5 shows the switching characteristics of a simplified clamped-inductive-switching circuit. The controllable switch is connected with a constant current load [20]. The dashed areas are the switching losses.

2.3.1. Modeling of MOSFET or IGBT Loss

The MOSFET or IGBT losses (P_Q) can be calculated by

$$P_Q = P_{cond,Q} + P_{sw,Q} \,. \tag{2.32}$$

The conduction losses for MOSFET or IGBT can be expressed as

$$P_{cond,Q} = I_{Q,ave} V_{CE} + I_{Q,rms}^2 R_{CE,on} \,. \tag{2.33}$$

According to [25][26], if the converter controller is assumed to be of a sinusoidal *pulse-width modulation* (PWM) type, the energy loss of the IGBT or MOSFET (W_Q) during the conduction period is

$$W_Q = v_{CE} i_c D\tau \,. \tag{2.34}$$

The duty cycle in (2.34) is a function of current angles as is shown in [25][26]

$$D = \frac{1}{2}\left(1 + Msin(\theta_n)\right) = \frac{1}{2}\left(1 + Msin\left(\frac{2 * \pi * n}{N}\right)\right). \tag{2.35}$$

The collector current (i_c) is assumed to be sinusoidal, thus using (2.34) and (2.35), the energy loss during conduction is

$$W_Q = v_{CE} I_c sin(\alpha) \frac{1}{2}\left(1 + Msin(\theta_n)\right)\tau \,. \tag{2.36}$$

The total energy loss in (2.36) will remain the same if the number of pulses increases [25]. Therefore, (2.36) may be converted to a differential equation. The average energy in a cycle is an integral of the differential energy during half of a period. The power will be the average energy divided by the full period as expressed below:

$$P_{cond,Q} = \left(\frac{1}{8} + \frac{M}{3\pi} cos(\theta)\right) R_{CE,on} I_Q^2 + \left(\frac{1}{2\pi} + \frac{M}{8} cos(\theta)\right) I_Q V_{CE} \,. \tag{2.37}$$

From Figure 2.5, the dissipated energy in the switching devices during the turn-on and turn-off can be approximated in the dashed area. The dashed area is assumed to be a perfect triangle. Therefore, the average switching losses can be calculated using [20]

$$P_{sw,Q} = \frac{V_Q I_Q}{2} f_{sw}\left(t_{on,sw} + t_{off,sw}\right) \,. \tag{2.38}$$

The above equation is load-dependent. The average switching losses depend linearly on the switching frequency and the switching times (turn-on and turn-off time). Therefore, the total losses for the MOSFET or IGBT are

$$\begin{aligned} P_Q = &\left(\frac{1}{8} + \frac{M}{3\pi} cos(\theta)\right) R_{CE,on} I_Q^2 + \left(\frac{1}{2\pi} + \frac{M}{8} cos(\theta)\right) I_Q V_{CE} \\ &+ \frac{V_Q I_Q}{2} f_{sw}\left(t_{on,sw} + t_{off,sw}\right) \,. \end{aligned} \tag{2.39}$$

2.3.2. Modeling of Power Diode Loss

The anti-parallel power diode losses have two main parts: conduction and switching losses. Calculation of the conduction losses is almost the same with the losses in the MOSFET, except that the duty cycle of the anti-parallel power diode is different [25]-[26] due to different times of their

operation. The anti-parallel power diodes will conduct when the current flowing through the diode is positive, while at the same time the MOSFET or IGBT is off. So, the conduction losses for the anti-parallel power diode can be calculated using the expression

$$P_{cond,D} = \left(\frac{1}{8} - \frac{M}{3\pi}cos(\theta)\right)R_{D,on}I_D^2 + \left(\frac{1}{2\pi} - \frac{M}{8}cos(\theta)\right)I_D V_D. \tag{2.40}$$

The most important parameter in the diode switching losses is the reverse recovery losses [10][20], while the rest of losses can be neglected. The switching waveform of the power diode can be seen in Figure 2.6. The switching losses of the diode can be expressed by

$$P_{sw,D} = \frac{f_{sw}V_R}{2S}\left(\frac{dI_F}{dt}\right)\left(\frac{St_{rr}}{S+1}\right)^2. \tag{2.41}$$

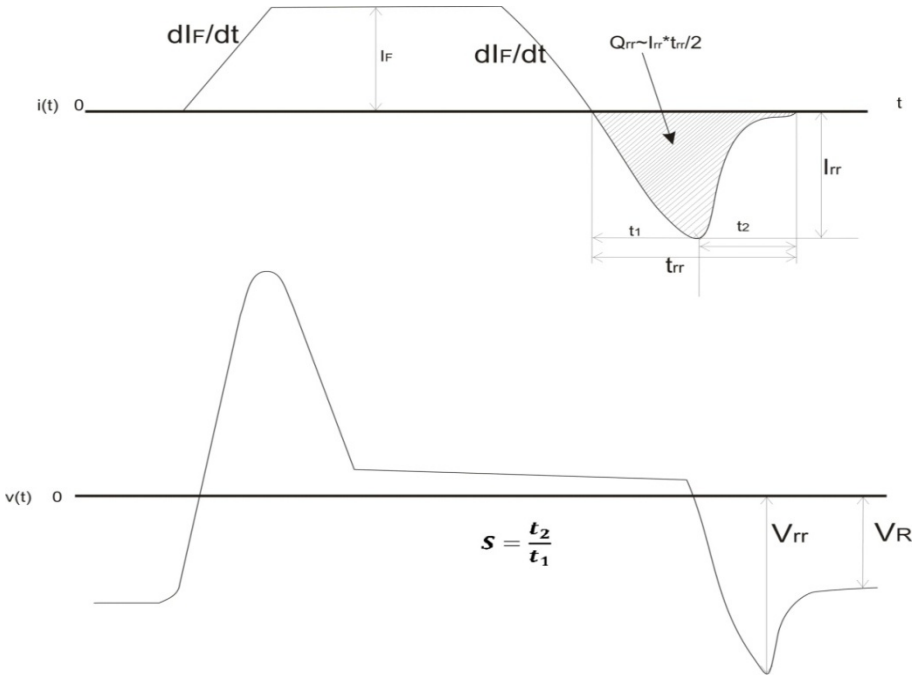

Figure 2.6 Switching waveform of the power diode

The power electronic converter schematic for a four-quadrant speed controlled induction motor can be assumed to be the same converter as in Figure 2.7 and has the capability of transferring a regenerative braking energy. The power electronic converter losses (P_{PEC}) in (2.39) - (2.41) must be multiplied by 6 due to the number of the MOSFETs and anti-parallel power diodes in the power electronic converter.

$$P_{PEC} = 6\left(P_{cond,Q} + P_{sw,Q}\right) + 6\left(P_{cond,D} + P_{sw,D}\right). \tag{2.42}$$

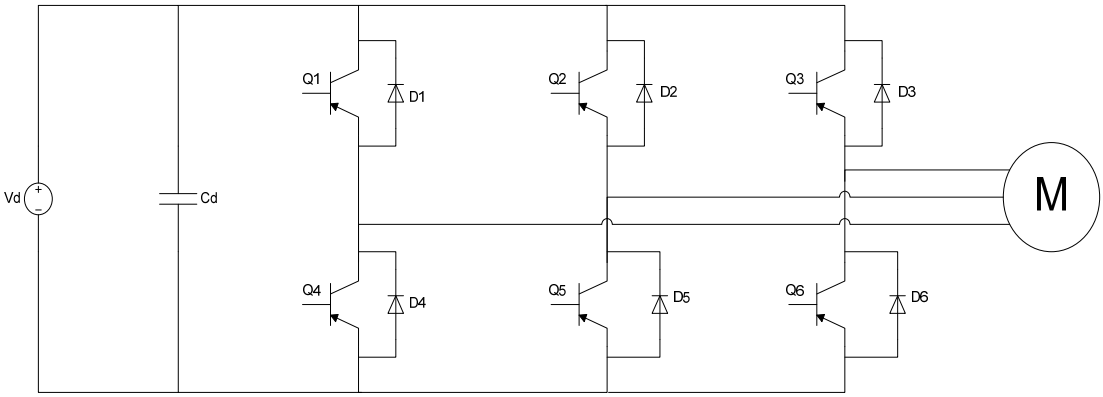

Figure 2.7 Three-phase inverter for Induction motor

2.4. Modeling of Battery

A battery is a device that converts chemical energy into electrical energy and vice versa. Complete modeling of a battery is a very complex procedure and requires thorough knowledge of electrochemistry. One common type of battery models is electric circuit-based battery model that represents an electrical characteristic of the battery. There are many types of electric circuit-based battery models as reported in [27] - [30].

Some general terms and terminologies used in battery modeling are C-rates, state of charge (SOC), open circuit voltage, cut-off voltage (end of nominal zone), nominal voltage, and battery capacity.

C-rate means the discharge current in order to normalize against the battery capacity. It is used as a measure of the rate at which the battery is discharged relative to its maximum capacity. For example, a 1C rate means that the discharge current will discharge the entire battery in 1 hour. For a battery with a capacity of 100 Amp-hrs, this equates to a discharge current of 100 Amps. A 5C rate for this battery would be 500 Amps, and a C/2 rate would be 50 Amps. In reality, high C rate result in even lower discharge times. SOC is an expression of the present battery capacity as a percentage of maximum capacity. SOC is generally calculated using current integration to determine the change in the battery capacity over time. An open circuit voltage is the voltage at the battery terminals with no load applied. The open-circuit voltage depends on the SOC of battery.

In this thesis, a generic battery model will be used. The model is a modification of the Sheppard discharge battery model introduced by [30]. The battery is modeled using a controlled voltage source in series with constant internal resistance, as shown in Figure 2.8. This model is based on several assumptions:

- the model has the same characteristic of charge and discharge cycles
- the model has constant internal resistance
- there is no Peukert effect; the battery capacity does not change with the amplitude of the current.

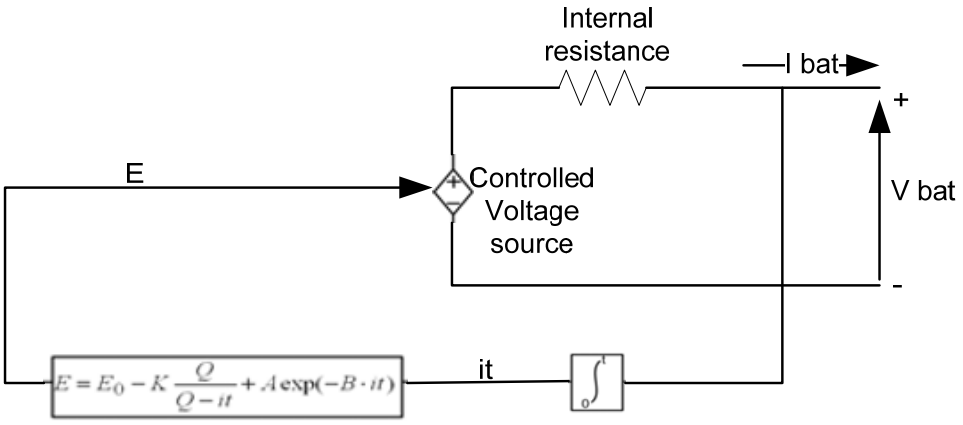

Figure 2.8 Generic battery model

The open-circuit voltage sources are calculated with a non-linear equation based on the actual SOC of the battery as follows:

$$E = E_o - K\left(\frac{Q}{Q-\int idt}\right)i + Ae^{(-B\int idt)} \tag{2.43}$$

This model can represent the behavior of different battery types. The parameters of this model can be extracted from the discharge curve data or datasheet from the manufacturer by the following steps.

Internal resistance approximation represents the voltage drop in the battery caused by current variation. Usually, the internal resistance is specified in the manufacturer's datasheet. It can also be calculated from the potential difference caused by current variation.

Model parameter is derived from the typical discharge curve from manufacture which can be used to calculate the unknown parameter in (2.43). In the discharge curve, there are a full-charge voltage, an end of the exponential zone (voltage and charge) and an end of the nominal zone (voltage and charge).

A : voltage drop during the exponential zone (V)

$$A = E_{full} - E_{Exp} \tag{2.44}$$

3/(B) : charge at the end of exponential zone (Ah)

$$B = \frac{3}{Q_{Exp}} \tag{2.45}$$

$$K = \frac{\left(E_{Full} - E_{Nom} + A(e^{-B.Q_{Nom}}) - 1\right).(Q - Q_{Nom})}{Q_{Nom}}. \tag{2.46}$$

And then, the voltage constant (E_o) is deducted from the fully charged voltage (E_{Full}):

$$E_o = E_{Full} + K + R_{in}i_{bat} - A \tag{2.47}$$

2.5. Regenerative Braking

Regenerative braking is a mechanism to reduce the vehicle speed by converting some of its kinetic energy to other useful form of energy [31]-[33]. This converted energy can be used to charge

the energy storage in the system, such as a battery or a capacitor. The regenerative braking is different from an auxiliary drive braking, where the electrical energy is dissipated as heat by passing current through large bank of variable resistors.

Regenerative braking does not have a sufficient effect in lowering the speed. Therefore, a friction brake is still required as complete brake and back-up brake. The total energy dissipation is limited by either the capacity of the supply system to absorb this energy or by the SOC of the battery. If SOC of the battery is full, the auxiliary drive braking will absorb the excess energy. In regenerative braking, the electric motor acts as generator and transfers the energy to the energy storage which provides braking effect as can be seen in Figure 2.10. In order to capture the regenerative braking energy, the total traction torque must be negative.

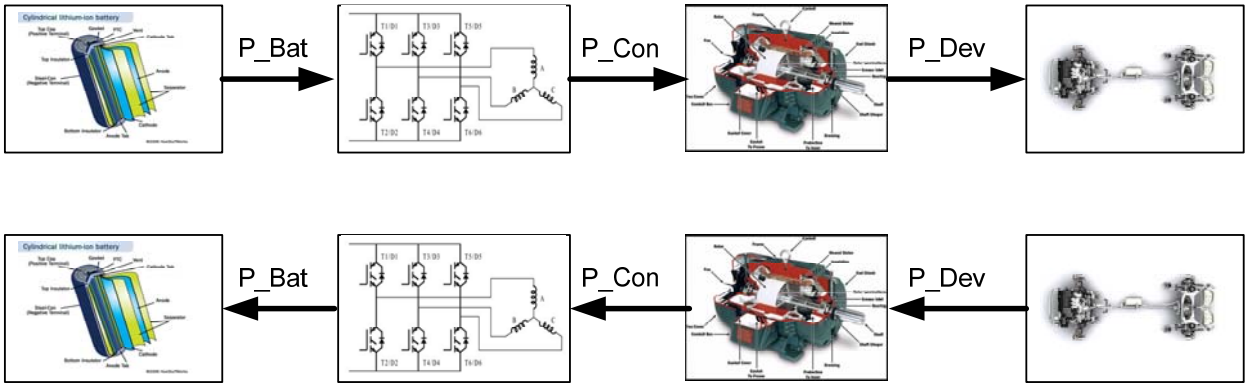

Figure 2.10 Normal (above) and regenerative braking (below) operation of electric traction drive system

The efficiency of these systems can be seen in Table 2.1:

Table 2.1
Comparison of normal and regenerative braking efficiency of drive system

Component	Normal propulsion	Regenerative braking
Battery	$\eta_{Battery} = \frac{P_{Bat}}{P_{bat\_in}}$	$\eta_{Battery} = \frac{P_{bat\_in}}{P_{Bat}}$
Converter	$\eta_{converter} = \frac{P_{Bat}}{P_{Con}}$	$\eta_{converter} = \frac{P_{Con}}{P_{Bat}}$
Electric motor	$\eta_{motor} = \frac{P_{Con}}{P_{Dev}}$	$\eta_{motor} = \frac{P_{Dev}}{P_{Con}}$

3. LOAD PROFILE OF THE ELECTRIC TRACTION DRIVE SYSTEM

This chapter describes the profile of load input used in the thesis. The basic steps of selecting components in the electric traction drive system are presented.

3.1. Load profile of the electric traction drive system

The load used in this thesis was drive cycle of ICE karting at race day for one lap (48 seconds). This drive cycle had previously been measured by the *Flap track* software at Göteborg karting ring track. The speed profile of the ICE karting for one lap can be seen in Figure 3.1.

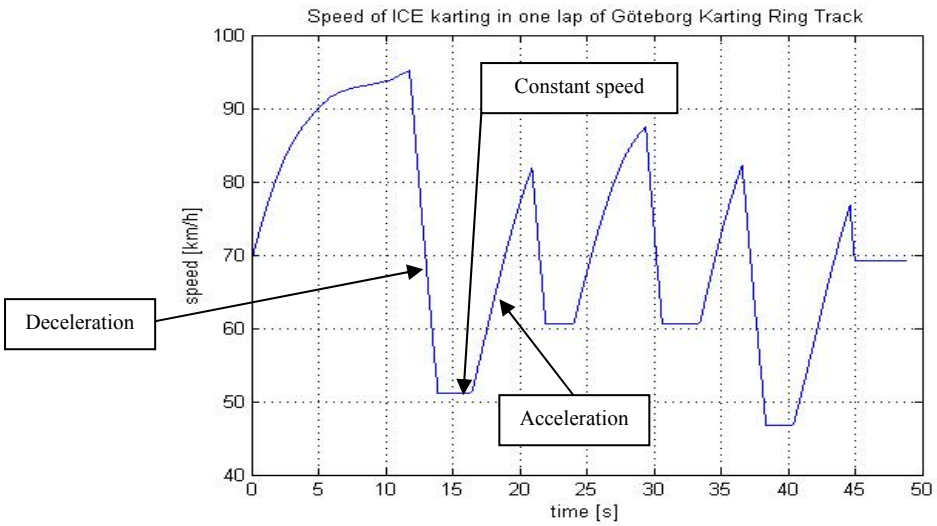

Figure 3.1 Speed profile of ICE karting at Göteborg karting ring track

From Figure 3.1, it is clear that the ICE karting has high acceleration and deceleration. In order to use this speed profile as an input in the simulation, the speed profile (km/h) in Figure 3.1 must be converted into another speed profile (rad/s) using (3.1). The result can be seen in Figure 3.2.

$$\omega_t = \frac{10v}{36r}. \tag{3.1}$$

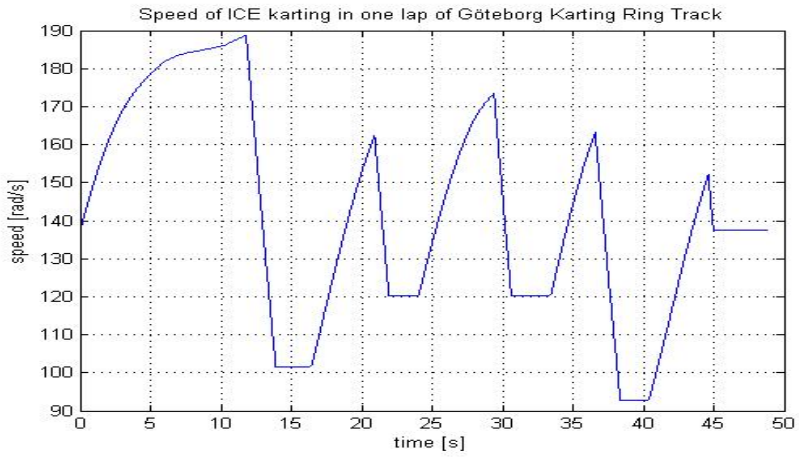

Figure 3.2 Speed profile of ICE karting at Göteborg karting ring track in rad/sec

From Figure 3.2, the characteristics of the speed profile can be described as follows:

- the maximum angular speed is 189 rad/s
- the lowest angular speed is 93 rad/s
- the initial speed is 138 rad/s.

These speed characteristics must be changed to rpm by (3.2). The values are 1802 rpm for the maximum angular speed and 885 rpm for the minimum angular speed.

$$v_{rpm} = \frac{\omega_t}{\frac{2\pi}{60}}. \tag{3.2}$$

According to this speed characteristics, the electric traction torque of the electric karting is calculated using (2.1) - (2.6) described in Section 2.1. In this thesis, the calculation was accomplished using Matlab® scripts. The results were the torque and acceleration profiles at a wheel of the ICE karting, which are shown in Figure 3.3.

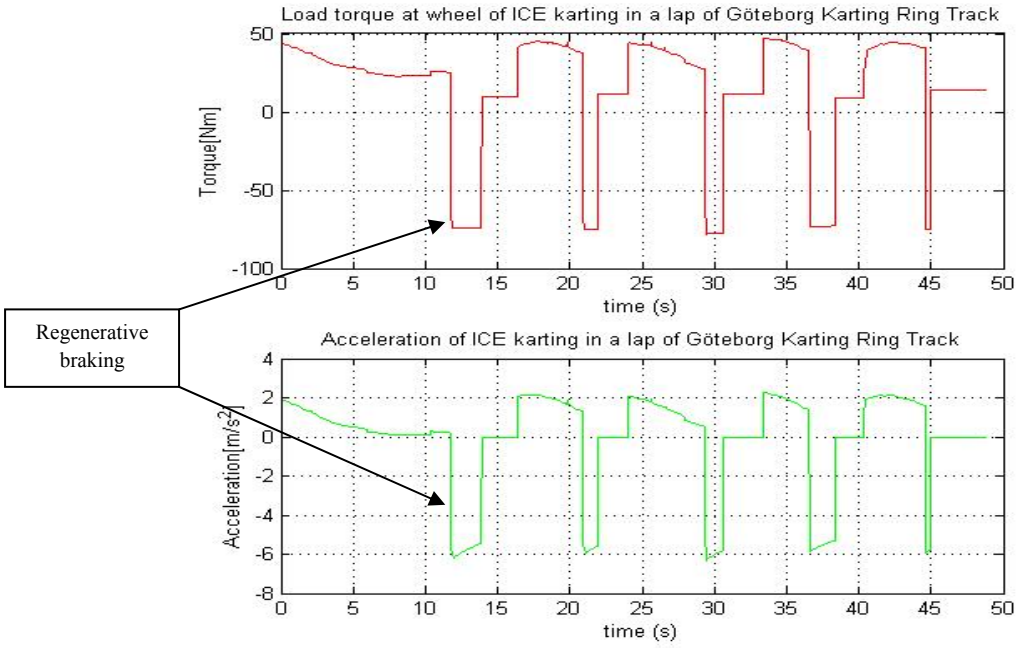

Figure 3.3 Load profile and acceleration of go-kart at Göteborg karting ring track

The traction torque at the wheel is varying between 47 Nm and -78 Nm. The negative torque indicates that the ICE karting is in deceleration or in regenerative braking region. It is clear that the regenerative braking or deceleration torque is higher than the acceleration torque. Therefore, the regenerative power used in charging the battery must be limited due to the limitation of the electric motor, power electronic converter and battery capability [32].

The power required to run the ICE karting is calculated from the speed and torque profile in Figure 3.2 and 3.3 and by using (2.5). Figure 3.4 shows the power requirement of the ICE karting with and without the regenerative power. It is shown that the maximum regenerative power is higher than the maximum acceleration power. The energy used to run the ICE karting in this drive cycle is 30 Wh and 48.7 Wh for the case with and without the regenerative power.

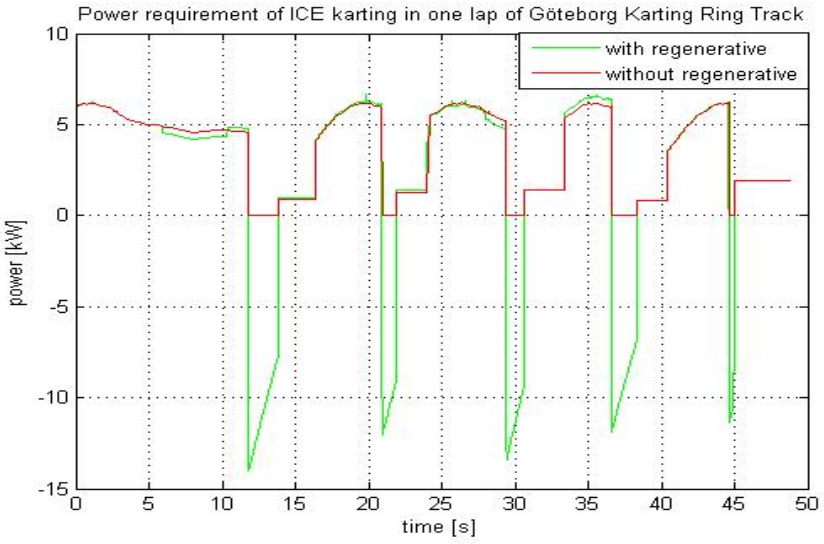

Figure 3.4 power profile of go-kart at Göteborg karting ring track

3.2. Selecting Drive Components

An electric traction drive system for electric karting consists of a vehicle transmission system, an electric motor, a power electronic converter, an energy storage system (battery), and a controller. To design the electric traction drive system for electric karting, the basic requirements to get the optimum solution for all the components must be achieved.

3.2.1. Match between the electric motor and vehicle transmission system

The type of the electric motor used in this thesis is selected based on power rating, speed of operation, operating environment, reliability, performance requirements by the load, and costs of overall drives.

The electric motor should be able to handle the load (vehicle transmission system) if the rated characteristics of the electric motor match the load characteristics. The load parameters, such as load inertia, maximum speed, speed range, and direction of motion, must first be known [20]. From those parameters, the total electromagnetic torque required by the electric motor can be calculated using (2.8).

The load torque is the total traction torques of the electric karting as described in Section 2.1. The developed power in the electric motor that is required for this load can be found using the relation

$$P_d = T_d \omega_r \tag{3.3}$$

From the load-torque profile in Figure 3.3, the motor current-profile can also be calculated by the torque and stator or armature current correlation described in Chapter 2. This relation is different for each type of electric motor [14], [15]. For example, the stator current of the motor is proportional to the electromagnetic torque for a permanent magnet DC motor if the flux in the air gap of the motor is kept constant. Normally, there is a gearing mechanism between the electric motor and the load. The gear mechanism can provide the peak torque at specified speeds.

The power needed to run the electric motor can be seen in Figure 3.4. This figure shows that the maximum power of the load profile is 6.67 kW for less than 1 second, the minimum power is 0 kW and the average power without the regenerative braking power is 3.6 kW. If the efficiency of the transmission is assumed to be 100% and the efficiency of the motor is assumed to be 70%, the power rating of the electric motor must be higher than 5.2 kW. The maximum power in the regenerative braking is 14 kW for less than 1 second. Therefore, the regenerative braking power that will be used to recharge the battery must be limited to the maximum power of the electric motor, power electronic converter and battery. The used energy in the transmission without the regenerative braking power is 0.049 kWh in 48 seconds. If the regenerative braking energy is used for recharging the battery, the total energy in the transmission is 0.03 kWh for 48 seconds.

3.2.2. Match between the electric motor and the power electronic converter

The selection of the power electronic converter topology and its controller depends on the selected type of a motor drive. The output of the power electronic converter is a controlled voltage that will be used to control the motor current and electromagnetic torque. Based on this output, some considerations in choosing the power electronic converter must be fulfilled.

Firstly, the current rating of the power electronic converter must be selected based on both the rms and the peak values of the required stator current. The thermal characteristic of the power electronic converter also needs to be considered because the current will produce losses in the power electronic converter and the controller. These losses will increase the temperature, while the power electronic converter has a limited range of operating temperature. Generally, the minimum rated current and voltage of the power electronic converter should be the same as for the electric motor.

The rated voltage of the power electronic converter is used to control the motor current and also the torque. Therefore, the output of the power electronic converter must be larger than the electromotive force voltage (e). The difference of the electromotive force voltage of the electric motor and the output of the power electronic converter produce the current and the current ripple as shown below.

$$\frac{di}{dt} = \frac{v - e}{L} \tag{3.4}$$

The electromotive force voltage of the electric motor increases linearly with the motor speed, assuming a constant flux in the air gap of the motor. Therefore, the voltage rating of the converter depends on the maximum motor speed assuming a constant air gap flux.

The switching frequency and the motor inductance must be considered for the selection of the power electronic converter. The motor inductance will affect the motor current ripple; higher ripple will produce higher losses. The choice of switching frequency would affect the switching losses but could also be used to reduce the ripple motor current.

From the load profile in Figure 3.3, the rms and average current rating of the power rating used in this thesis must be in the range of 75 - 160 Ampere, with variable output voltages. The converter is of 4-quadrant type, has the power of 5.5 kW and switching frequency of 10 kHz.

3.2.3. Match between the power electronics converter and battery

Generally, selection of the battery depends on the battery performance. The factors that affect the battery performance are state of charge (SOC), battery storage capacity, rate of discharge/charge, temperature, internal resistance and lifetime. These parameters are listed in Appendix.

According to the power profile of the go kart in Figure 3.3, the energy required to run the electric karting using the battery is around 49 Wh or 1.015 Ah (the battery voltage is 48 Vdc) for 48 seconds. Therefore, to operate for 13 minutes, the battery capacity must be larger than 16.5 Ah.

4. EXPERIMENT SETUP

This chapter describes the experiment setup for measuring the parameters of the induction motor and battery.

4.1. Measurement Setup for the Induction Motor

In order to find the parameters of the induction motor (R_r, L_r, L_s, L_m, and R_m) in Figure 2.7, a no-load test and a locked rotor test must be performed. Stator resistance can be found by measuring the line-to-line stator winding resistance. Per-phase stator resistance is one half of line-to-line stator winding resistance.

Diagram of the measurement setup can be seen in Figure 4.1.

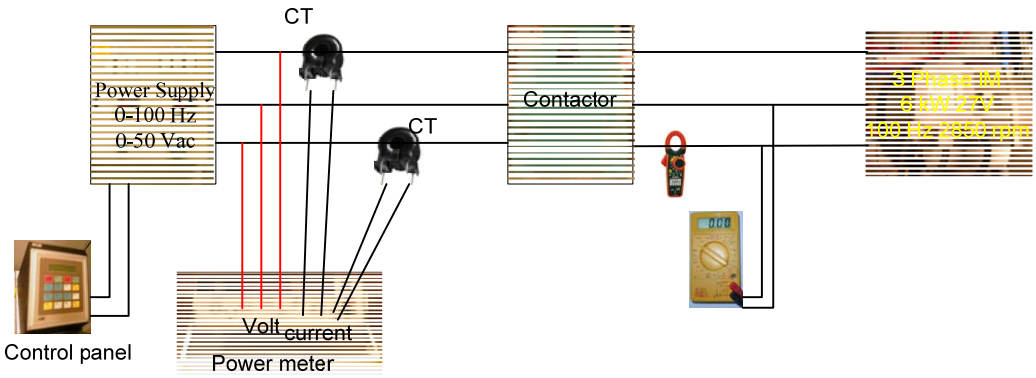

Figure 4.1 Measurement setup of the induction motor

The rating of the induction motor used in this thesis can be seen in Table 4.1

Table 4.1
Induction Motor Rating

Power	6000	W
Voltage	3 x 27	V
Frequency	100	Hz
Speed	2850	rpm
Current	168	A
Weight	19.2	kg

4.1.1. No-Load Test

No-load test is used to measure copper losses at stator winding, core losses and mechanical losses [35]-[36]. This test is done by operating the motor at rated voltage and frequency without a load connected to the rotor shaft. At this condition, the slip (s) approximately equals zero and the rotor resistance $\frac{R_r}{s}$ is infinite. Therefore, the rotor inductance and resistance can be ignored. The equivalent circuit for the test can be seen in Figure 4.2.

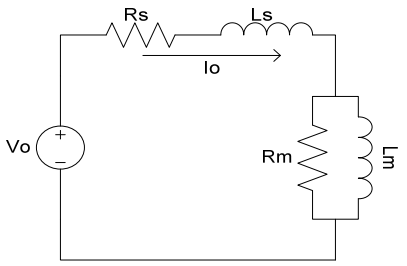

Figure 4.2 Equivalent circuit of the induction motor at no-load test

In this test, the no-load input power, no-load line current, and phase voltage are measured at rated frequency. The input voltages are ranging from 125 % of the rated voltage down to the voltage where further voltage reduction increases the line current.

Stator losses can be calculated by

$$P_{cus} = 3I_o^2 R_s \,. \tag{4.1}$$

The mechanical losses can be calculated by performing a linear regression analysis of the power-versus-voltage-square curve. The curve can be constructed by subtracting the stator losses from total no-load losses at each test voltage points, and then extending the curve to zero voltage. The intersection with the Y-axis gives the mechanical losses. The core loss at each test voltage can be found by subtracting stator and mechanical losses from the total no-load losses.

From Figure 4.2, the total impedance of the induction motor at no-load test condition can be found by

$$Z_m = \frac{jR_m X_m}{R_m + jX_m} = \frac{jR_m X_m (R_m - jX_m)}{R_m^2 + X_m^2}. \tag{4.2}$$

It is assumed that the value of $X_m^2 \ll R_m^2$, (4.2) becomes

$$Z_m \approx jX_m + \frac{X_m^2}{R_m}. \tag{4.3}$$

Then the total impedance in no-load test is

$$Z_o = R_s + \frac{X_m^2}{R_m} + j(X_m + X_s)\,. \tag{4.4}$$

The phase angle between voltage and current at no-load test can be calculated using

$$\theta_o = arccos\left(\frac{P_o}{3\left(\frac{V_o}{\sqrt{3}}\right)I_o}\right). \tag{4.5}$$

The magnitude of total impedance in no-load test can be calculated using

$$Z_o = \frac{\left|\frac{V_o}{\sqrt{3}}\right|}{|I_o|}. \tag{4.6}$$

Real and imaginary inductances can be calculated using

$$X_m + X_s = \Im\left(\frac{\frac{V_o}{\sqrt{3}}}{I_o}\right) = Z_o sin(\theta_o) \tag{4.7}$$

$$R_s + \frac{X_m^2}{R_m} = \Re\left(\frac{\frac{V_o}{\sqrt{3}}}{I_o}\right) = Z_o cos(\theta_o)\,. \tag{4.8}$$

4.1.2. Locked Rotor Test

The locked rotor test can be performed by operating the induction motor at one or more frequencies and voltages. The test shall be conducted at rated current. The value of the impedance used in the equivalent circuit calculation is at the exact value of saturation and deep bar effect. Otherwise, the calculated power factor will be found to be higher than the true value [35]. The impedance shall be measured at the temperature of the motor at the time of the test. In this test the value of power input, current and voltage are measured. It is assumed that no core losses occur. The equivalent circuit of locked rotor test can be seen in Figure 4.3.

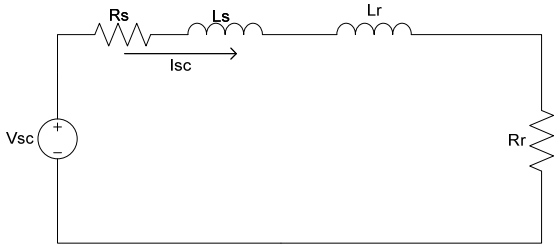

Figure 4.3 Equivalent circuit of induction motor at locked rotor test

From Figure 4.3, the total impedance in locked rotor test can be calculated by

$$Z_{sc} = R_s + R_r + j(X_r + X_s). \tag{4.9}$$

The phase angle between voltage and current at locked rotor test can be found similarly from no-load test. Stator and rotor inductance can be calculated by

$$X_r + X_s = \Im\left(\frac{\frac{V_{sc}}{\sqrt{3}}}{I_{sc}}\right) = Z_{sc} sin(\theta_{sc})\,. \tag{4.10}$$

Rotor resistance can be calculated by

$$R_r = \Re\left(\frac{V_{sc}}{\sqrt{3}}\right) - R_s = Z_{sc} cos(\theta_{sc}) - R_s\,. \tag{4.11}$$

The result from (4.2) – (4.11) can be used as initial value to calculate the parameters of the induction motor according to [35].

First, reactive power at no-load and locked rotor test was calculated by

$$Q_o = \sqrt{\left(m\frac{V_o}{\sqrt{3}}I_o\right)^2 - P_o^2} \tag{4.12}$$

$$Q_{sc} = \sqrt{\left(m\frac{V_{sc}}{\sqrt{3}}I_{sc}\right)^2 - P_{sc}^2}\,. \tag{4.13}$$

Then, magnetizing reactance can be calculated by assuming the value of X_s and $\frac{X_s}{X_m}$ from the previous calculation.

$$X_m = \frac{m\left(\frac{V_o}{\sqrt{3}}\right)^2}{Q_o - (mI_o^2 X_s)}\,x\,\frac{1}{\left(1+\frac{X_s}{X_m}\right)^2}\,. \tag{4.14}$$

And stator leakage reactance at test frequency is calculated as

$$X_s = \frac{Q_{sc}}{mI_{sc}^2 x\left[1+\frac{X_s}{X_r}+\frac{X_s}{X_m}\right]}\,x\left[\frac{X_s}{X_r}+\frac{X_s}{X_m}\right]. \tag{4.15}$$

The result from (4.15) was used as input in (4.14) and this iterative solution was continued until the stable value of magnetizing and stator leakage reactance are obtained within 0.1% [35].

Secondly, rotor leakage reactance can be calculated by

$$X_r = \frac{X_s}{\frac{X_s}{X_r}}\,. \tag{4.15}$$

Core resistance can be calculated by

$$R_m = \frac{m\left(\frac{V_o}{\sqrt{3}}\right)^2}{P_{fe,o}\left(1+\frac{X_s}{X_m}\right)^2}\,. \tag{4.16}$$

Finally, rotor resistance can be calculated by

$$R_r = \left(\frac{P_{sc}}{mI_{sc}^2} - R_s\right)x\left(1+\frac{X_r}{X_m}\right)^2 - \left(\frac{X_r}{X_s}\right)^2 x\left(\frac{X_s^2}{R_m}\right). \tag{4.17}$$

4.1.3. Parameters of the Induction Motor

The result of the no-load and locked rotor test can be seen in Table 4.2 and 4.3.

Table 4.2
No-load test result

Voltage [V]	Current [A]	Power [W]
30.2	62	396
26.05	52.5	338
23.3	46.5	298
12.67	27	214

In Section 4.1.1, the mechanical losses can be found by Figure 4.4.

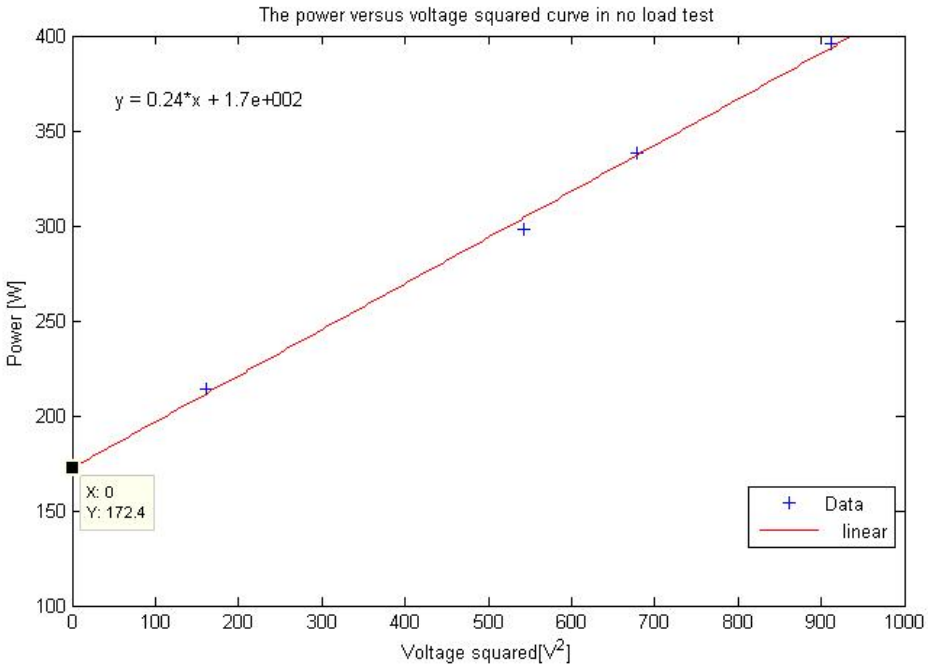

Figure 4.3 No-load test

From Figure 4.4, the intersection of the linear line (red line) and zero voltage (Y-axis) occurred at 172 W. Therefore, mechanical losses of the induction motor is 172 W and rated iron loss was 175 W.

Table 4.3
Locked rotor test result

Voltage [V]	Current [A]	Power [W]
3.7	70.5	192

The induction motor was assumed to be Design-A motor (ratio between the stator and rotor leakage reactance is one) and the test is done in ambient temperature. The parameters were calculated by MATLAB® script and the parameters of the induction motor can be seen in Table 4.4.

Table 4.4
Parameter of Induction motor

Stator resistance	0.0064 ohm
Rotor resistance	0.0071 ohm
Core resistance	6.5336 ohm
Stator leakage inductance	22.371 µH
Rotor leakage inductance	22.371 µH
Magnetizing inductance	0.43871 mH

4.2. Internal Resistance Battery Measurement

Internal resistance of the battery can be used to calculate the power losses in the battery. It is not possible to measure the internal resistance using an ohmmeter because the current generated by the battery itself will interfere with the measurement. There are several techniques that can be used to measure the internal resistance of the battery, such as a DC load test and an AC load test method. In this thesis, the DC load test was used to measure internal resistance due to the loss model and steady state analysis that was used in the simulation.

In the DC load test, open-circuit voltage and load voltage of the battery is measured. Then, a load was connected to the battery to have a current flow that leads to a reduced battery voltage, due to the IR voltage drop in the battery. The schematic of the DC load test can be seen in Figure 4.4. Figure 4.5 shows a photo of DC load test setup in laboratory. Internal resistance is calculated by Ohm laws from the voltage and current differences between two measurements.

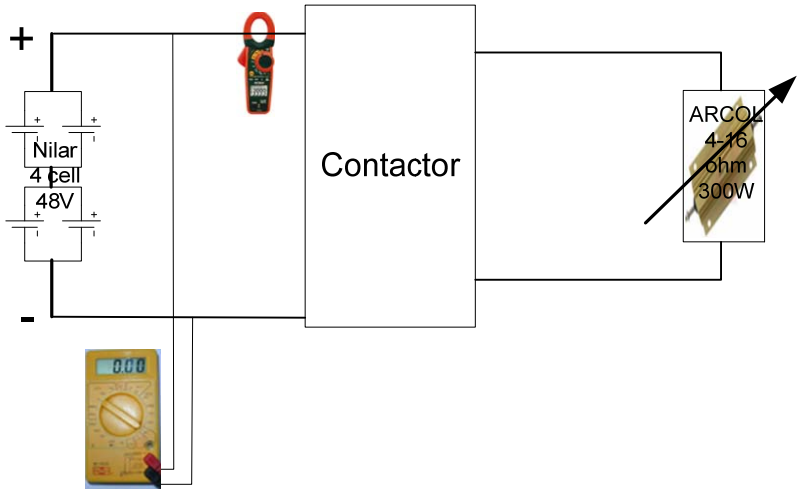

Figure 4.4 DC load test diagram of the battery

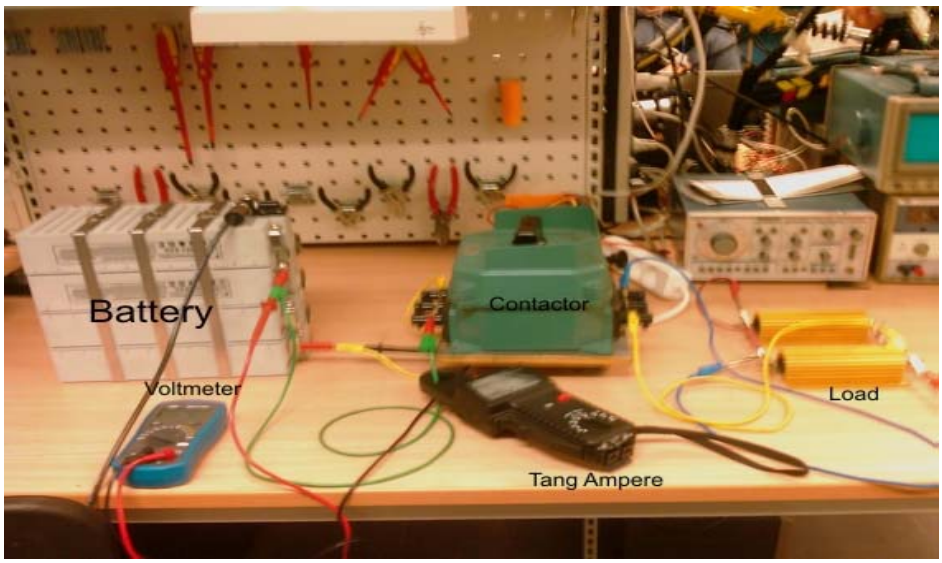

Figure 4.5 DC load test setup

Results of the measurement can be seen in Table 4.5.

Table 4.5
The DC load test measurement results

Voltage [V]	Current [A]	Rin [Ω]
48.9	0	
48.3	5.1	0.118
47.9	9.7	0.103
47.4	14.3	0.104

Internal resistance of the battery (R_{in}) can be found as

$$R_{in} = \frac{V_1 - V_2}{I_2 - I_1}. \tag{4.18}$$

According to the results in Table 4.5, average internal resistance of the batteries is 0.108Ω. The configuration of the batteries that were used in this test is shown in Figure 4.4. Therefore, internal resistance of each battery is 0.108 Ω.

5. MODELING THE ELECTRIC TRACTION DRIVE SYSTEM FOR ELECTRIC KARTING IN MATLAB®/SIMULINK®

In this chapter, the model of electric traction drive system components for electric karting described in Chapter 2 is implemented using Matlab®/Simulink®. A steady-state model is used to get raw data that is helpful during the design stage and for long-term analysis over an extended drive cycle. The advantage of this modeling is fast computation. The steady-state model is suitable to model the efficiency and performance of the system.

Based on the selected rating for the individual components of the electric karting drive system described in Chapter 3, the performance of each component can be modeled and computed separately.

5.1. Vehicles Dynamic Model

In this modeling, the drive cycle track is assumed to be flat. Therefore, the climbing resistance can be neglected and the total traction torque only depends on the rolling resistance, air drag resistance and acceleration resistance. The transmission block consists of all equations in Section 2.1. The inputs of this block are developed torque and moment inertia from the electric motor. The outputs are speed and position of the electric karting. The parameters of vehicle dynamics for a small electric karting can be seen in Table 5.1 and the vehicle dynamic model in Simulink® can be seen in Figure 5.1.

Table 5.1
Vehicle dynamic parameter for small go kart

Total mass	110	kg
Rolling resistance coefficient	0.03	
Drag coefficient	0.6	
Air density	1.202	kg/m^3
Vehicle cross section	0.5	m^2
Driving wheel radius	0.14	m

The total mass of the system for this simulation is assumed to be 110 kg, including the casing, driver, and the propulsion system (electric drive system). In air drag torque, the calculation is assumed to be not affected by wind speed. The initial speed in the integrator block is set at 138 rad/s.

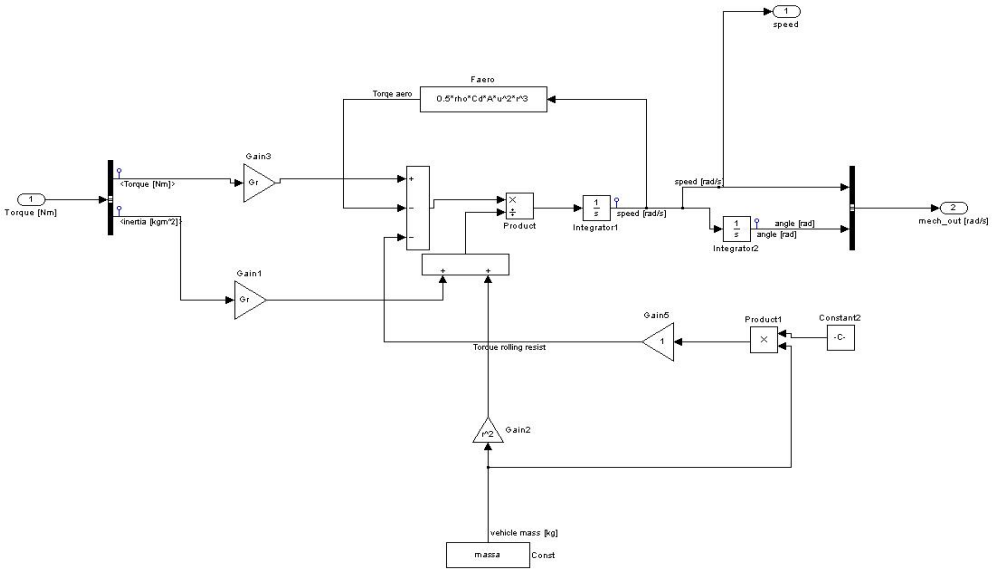

Figure 5.1 Simulink model for vehicle dynamic

5.2. Electric Motor Model

The model for the electric motor as seen in Figure 5.2 consists of two basic blocks: controller and loss model of electric motor block. The controller block is used to calculate the current in the stator, rotor, and the voltage drop in the air gap. The inputs of this block are torque and the speed in rad/s. In the other block as seen in Figure 5.3, the developed torque, losses and performance of the electric motor will be evaluated using (2.20), (2.26), and (2.31) in Section 2.2. Here, the regenerative braking will take action in the performance of the motor. As a result, in the loss model of the electric motor, there are two separate blocks to calculate efficiency of the electric motor at normal condition (as a motor) or regenerative braking (as generator). In normal condition, the calculations of efficiency use (2.31), but for the regenerative braking, the efficiency can be calculated using:

$$\eta_{motor} = \frac{T_d\omega_r - P_{loss}}{T_d\omega_r}\ x\ 100\%\ . \tag{5.1}$$

The inputs of this electric motor block are reference torque, electric karting speed from the vehicle dynamic model and voltage from the power electronic converter model. The outputs of this block are input electricity that contains stator current and power input of the electric motor, mechanical output that includes developed torque and moment inertia of the motor, motor performance that includes efficiency, developed output power, and power losses in the electric motor.

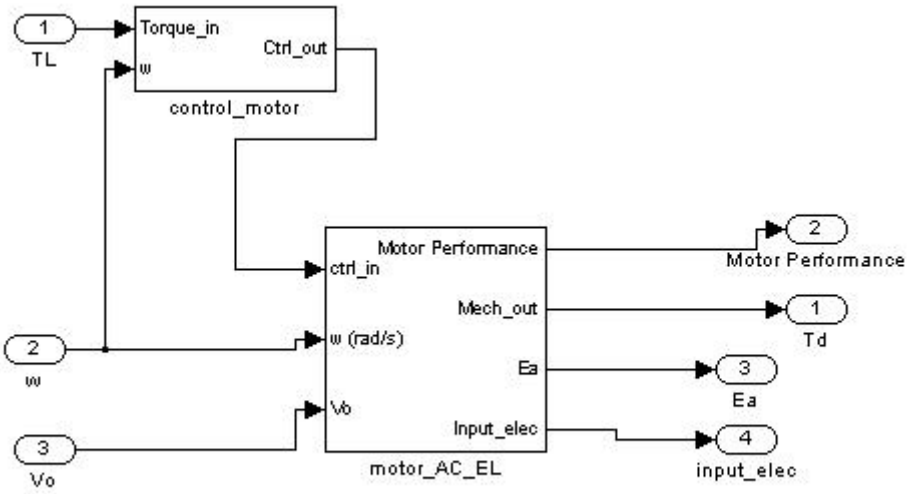

Figure 5.2 Simulink model for electric motor

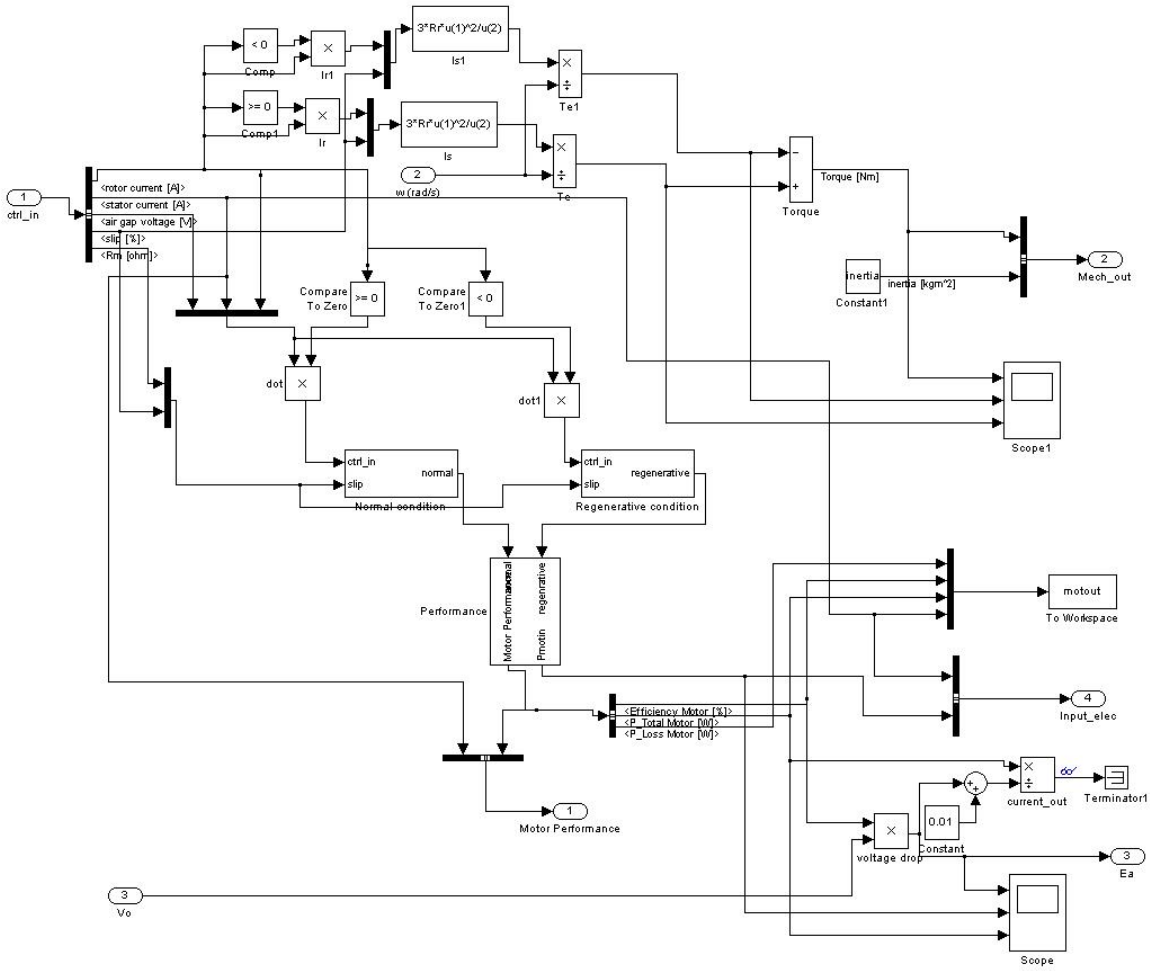

Figure 5.3 Simulink model for induction motor loss model

The simulation is assumed to be at constant flux operation and power factor at below the rated speed, thus the stator and rotor current can be assumed to be proportional to the output torque of the electric motor [21]. The parameters of this simulation can be found in Table 4.1 and 4.4.

The induction motor efficiency map can be seen in Figure 5.4. Above the rated speed, the voltage is limited. Therefore, the power is constant and torque is varying. Below the rated speed, the current is limited at rated torque. Therefore, the voltage and frequency were adjusted to give the constant maximum torque.

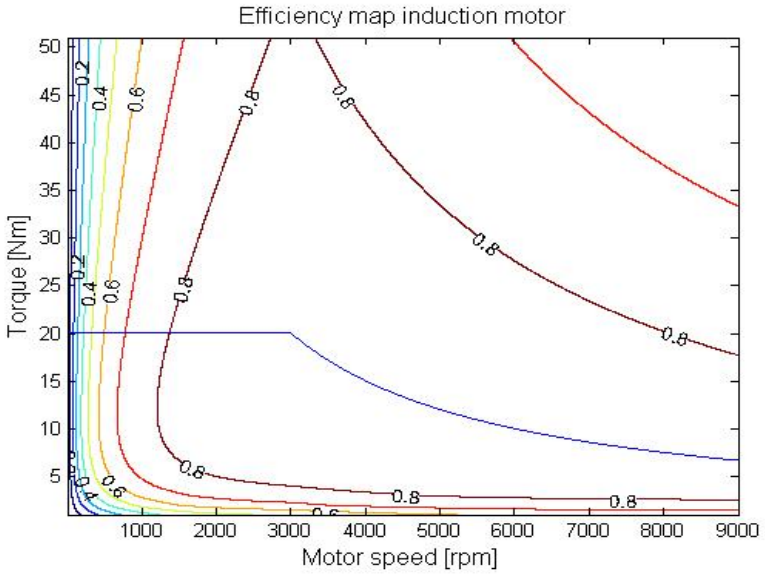

Figure 5.4 Efficiency maps for the used induction motor

The best performance was observed at points at around the rated value speed and above rated speed with lower rated torque. This is because copper and core losses decrease at higher speeds as can be seen in (2.29)-(2.30). However, if the speed increases up to two times the base speed, the performance decreases due to the increase of the winding and friction losses at higher speed [19] as described in (2.12) and the increase of the core loss due to the increasing electromotive force voltage as be seen in (2.25). At low speed, the torque is high, thus the performance of the induction motor was very low due to higher rotor and stator losses [19]-[22].

For the drive cycle as described at Chapter 3, the speed – power loss characteristic of the induction motor can be seen in Figure 5.5. Figure 5.5 shows that the induction motor loss decreases at above the rated speed and below the rated speed. The induction motor loss reaches the maximum at around the rated speed. At the constant power region (above the rated speed), the input voltage of the electric motor is not changed and the electromotive force voltage can be considered as increased. Hence, the stator and rotor loss decrease with an increase of frequency due to decreased the stator and rotor currents. The stator and rotor copper losses predominate (74%) in the induction motor loss.

The loss – transmitted power profile in the electric motor at the drive cycle used can be seen in Figure 5.6. It is clear that the regenerative braking condition, the power is larger than the power at normal condition. Therefore, the rotor, stator and iron losses are also higher in regenerative braking condition.

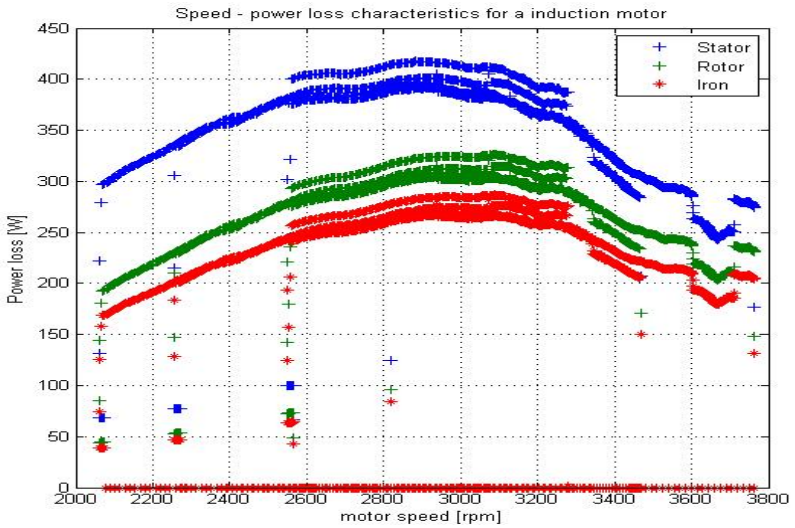

Figure 5.5 Speed – loss characteristic for the used induction motor in the used drive cycle

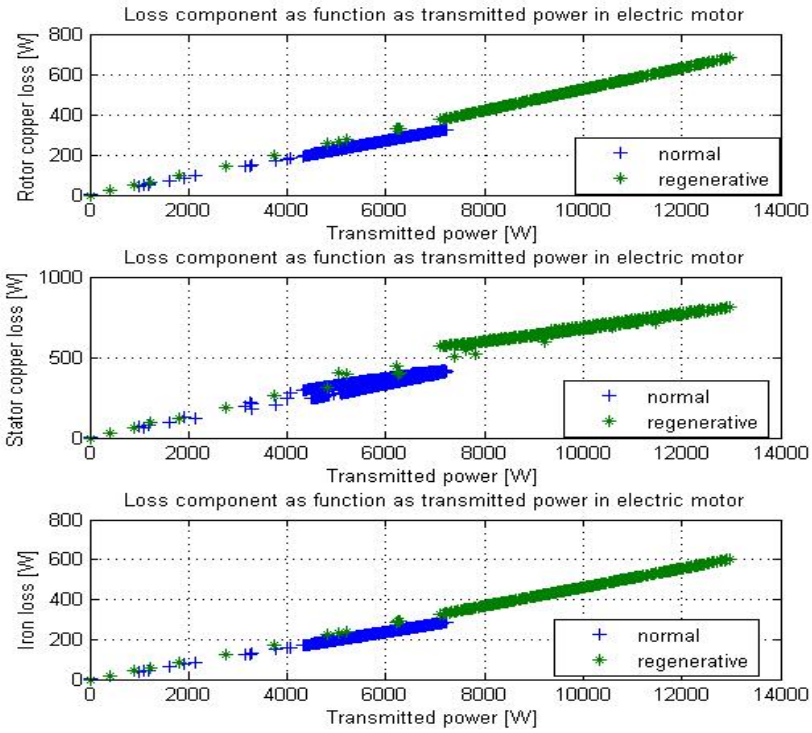

Figure 5.6 loss components as function of transmitted power for the used induction motor

From Figure 5.6, it can be seen that the stator, rotor and iron losses are proportional to the transmitted power in the electric motor. The electric motor loss increases with the transmitted power. To protect the motor insulation from the high increased temperature, the power from the regenerative braking should be limited [31]-[33].

5.3. Power Electronic Converter Model

The modeling for the power electronic converter is divided into two blocks, controller and full bridge as seen in Figure 5.7. The controller block is used to calculate rms and average current in the power diode and MOSFET that are described in Section 2.3.

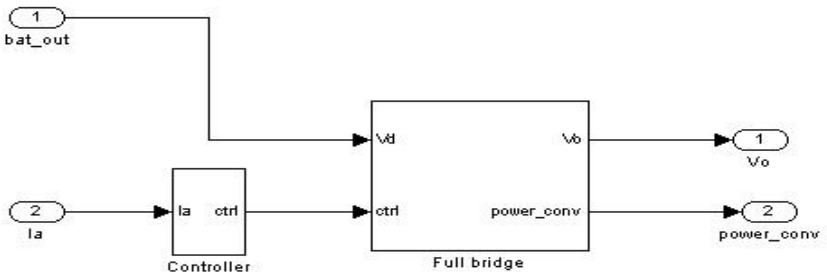

Figure 5.7 Simulink model for power electronics converter

The loss calculation was presented in the full bridge block that consists of conduction and switching losses for the power diode and the MOSFET. Similar with the electric motor, the regenerative braking also takes action in the calculation of the power electronic converter efficiency as seen in Figure 5.8.

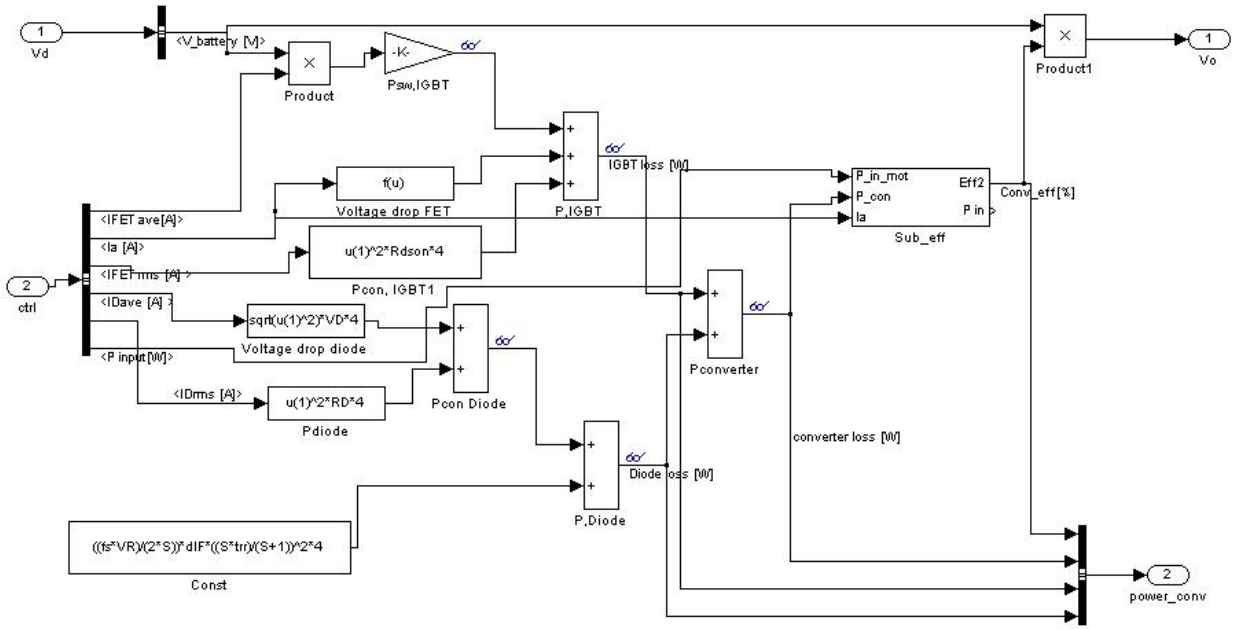

Figure 5.8 Simulink model for loss model power electronics converter

The efficiency of the converter in normal operation condition can be calculated using:

$$\eta_{converter} = \frac{P_{in\_motor}}{P_{in\_motor}+P_{loss}} x100\% \,. \tag{5.2}$$

And for regenerative braking condition:

$$\eta_{converter} = \frac{P_{in\_motor} - P_{loss}}{P_{in\_motor}} x100\% \,. \tag{5.3}$$

The inputs of the full bridge converter block are battery output that includes current and voltage from the battery, and stator current of the electric motor. The output of this block is voltage and performance of this converter that will be used to calculate the total performance of the system.

The parameters of the power electronic converter block can be found in Table 5.2.

Table 5.2
Power electronic converter parameter for the electric karting

Power MOSFET MTD3055VL		
Strain drain to source on-resistance	0.012	ohm
Rise time	85e-9	seconds
Fall time	43e-9	seconds
Constant voltage drop	0	V
Power Diode QuietIR series 20 ETF		
Forward voltage drop	1.2	V
On-resistance	0	ohm
rms reverse voltage	21	V
Snappiness factor	0.6	
Rate of fall forward current	100e6	A/s
Reverse recovery time	60e-9	seconds
Controller		
Frequency switching	10	kHz
Modulation index	0.5	
Power factor motor	0.8	

The result of the power electronic converter can be seen in Figure 5.9. The conduction losses make up a significant proportion of the total losses in the power electronic converter. The average conduction loss for the MOSFETs is 204 W and 158 W for the diodes. It is clear that the conduction losses are load-dependent and vary linearly with the square of the stator current of the electric motor. Therefore, the on-resistance of the MOSFET and the forward voltage drop in the power diode are the two main parameters that must be considered when choosing the power electronic component. The average switching losses in this converter is 7 W for the MOSFETs and 0.053 W for the diodes. It is clear that the switching loss for the diode is constant and independent of the output power, but the switching losses of the MOSFET is load-dependent and varies with the voltage and current.

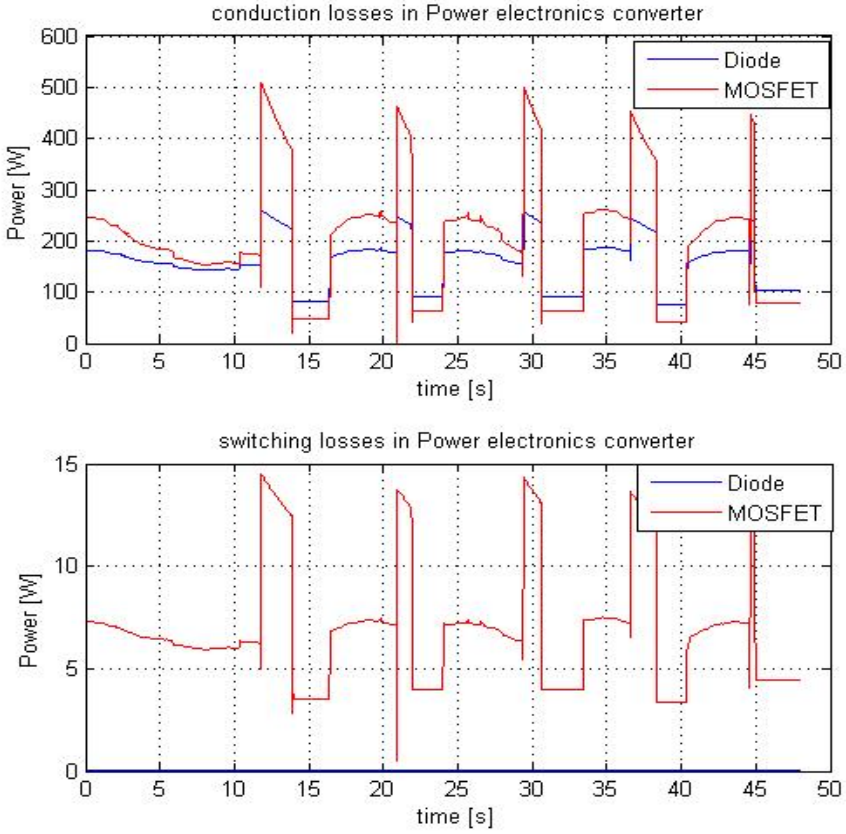

Figure 5.9 conduction and switching losses of power electronics converter

5.4. Battery Model

The battery model used in this simulation is a generic battery model that is described in Section 2.4 and shown in Figure 5.10. There are two blocks, SOC and battery performance, that are used to calculate the SOC and efficiency of the battery. The SOC of the battery can be calculated using:

$$SOC = 1 - \frac{it}{Q}. \tag{5.4}$$

The efficiency of the battery is the ratio of the power at the terminal battery to the open circuit power at the battery. The losses of the battery are dependent on the internal resistance of the battery and the current load of the battery. The limitation of regenerative braking and charging current allowed in the battery are set in integrator1 block. The parameters of the battery in (2.43) are:

Internal resistance, from the diagram of nominal current discharge characteristic of *Nilar membrane* battery, at the end of nominal zone point. The internal resistance battery (R_{in}) that will be used in the simulation can be calculated as

$$R_{in} = \frac{V_{C/20} - V_{1c}}{I} = \frac{25 - 23.2}{20} = 0.09\Omega\,. \tag{4.5}$$

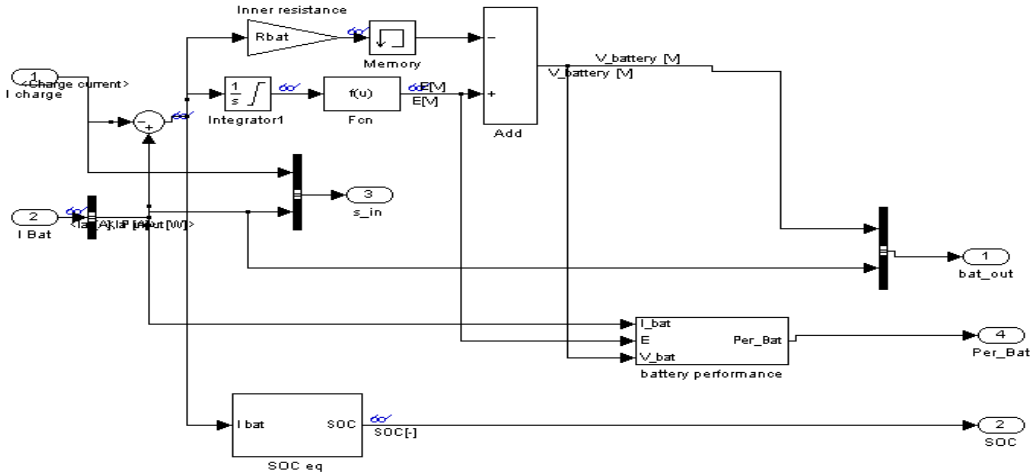

Figure 5.10 Simulink model for battery

Model parameter, by using (2.44)-(2.47), the discharge curve for *Nilar Membrane* battery can be extracted. The value of A is 2.6 V, B is 1.6667 $(Ah)^{-1}$, K =0.2286, and E_o is 26.473 V that was used in (2.43). From these parameters, the discharge curve of the *Nilar Membrane* Battery can be drawn as in Figure 5.11.

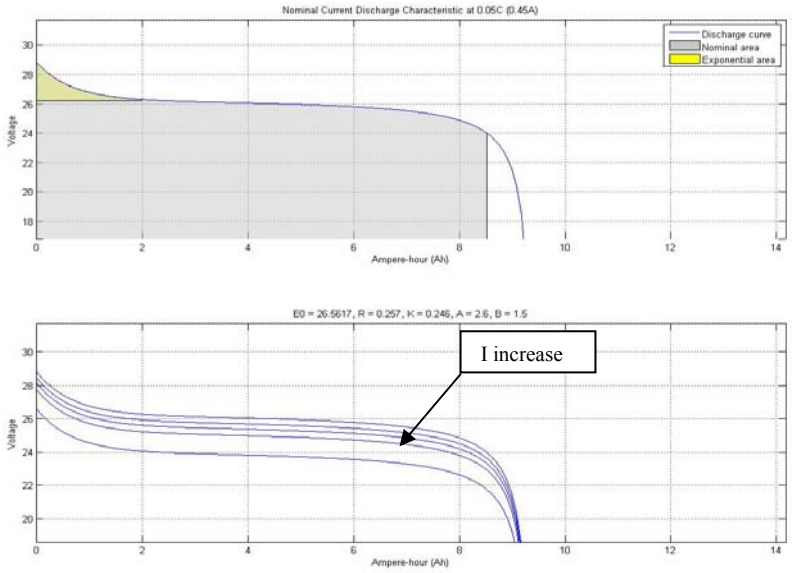

Figure 5.11 Discharge curve of Nilar membrane Battery

If the discharge current is 0.45 Ampere (0.05C), the output voltage of the battery is 26 V. The output voltage of the battery will decrease if the discharge current increases. At rated voltage of the battery (24V), the discharge current is 9A. The battery cannot operate below the end of nominal zone (cut-off voltage) [30].The weight of the battery is 3.9 kg.

5.5. Energy Conversion Block

This block presents the calculation of total efficiency of the system and total energy that was used for this electric karting and also the temperature variation as shown in figure 5.12.

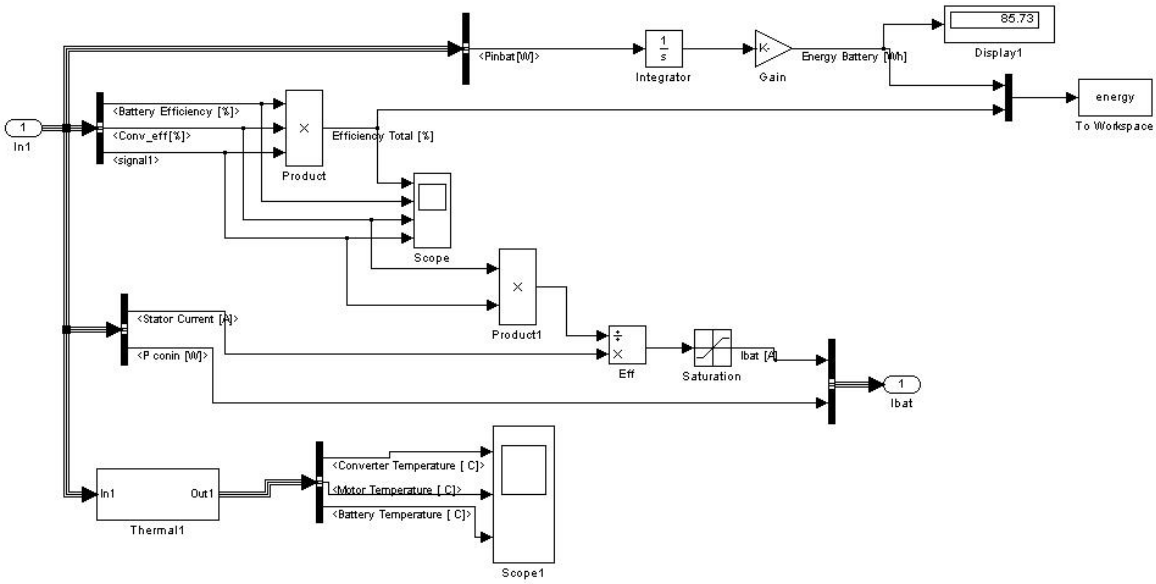

Figure 5.12 Simulink model for energy conversion block

5.6. Charging Block

The charging block is used to charge the battery from the line supply and has the power charger from the line and calculation of SOC that can be seen in figure 5.13.

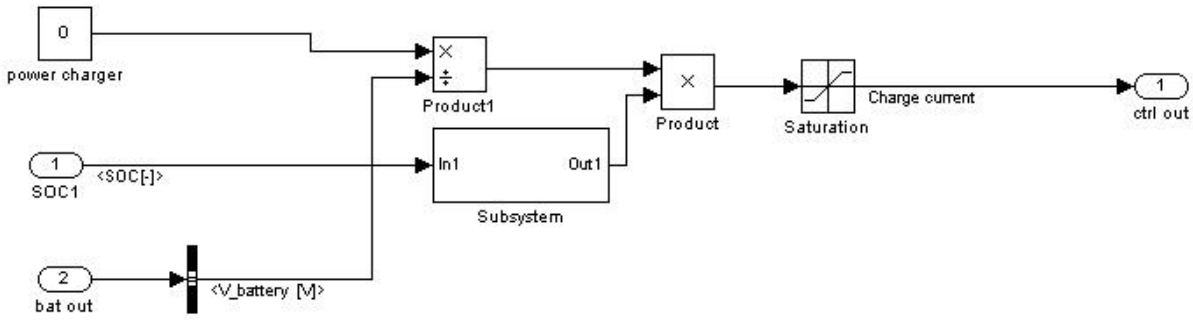

Figure 5.13 Simulink model for charging battery block

6. EVALUATION OF THE ELECTRIC TRACTION DRIVE SYSTEM FOR AN ELECTRIC KARTING APPLICATION

This chapter presents the simulation result of an electric traction drive system for an electric karting application. The efficiencies, power, energy usage and SOC of battery are presented and explained.

6.1. Overview the Electric Traction Drive System for Electric Karting

The separate models in Chapter 5 are integrated in MATLAB®/Simulink® to represent the complete model of the electric traction drive system. Figure 6.1 shows that the system's reference input is the load torque that represents the load profile of the drive cycle. There are six main blocks, each representing a component of the electric karting drive system. These blocks are already described in Chapters 2 and 5. The charger block is the block to charge the battery from the outside, but in this simulation it is assumed that there is no charging power from outside.

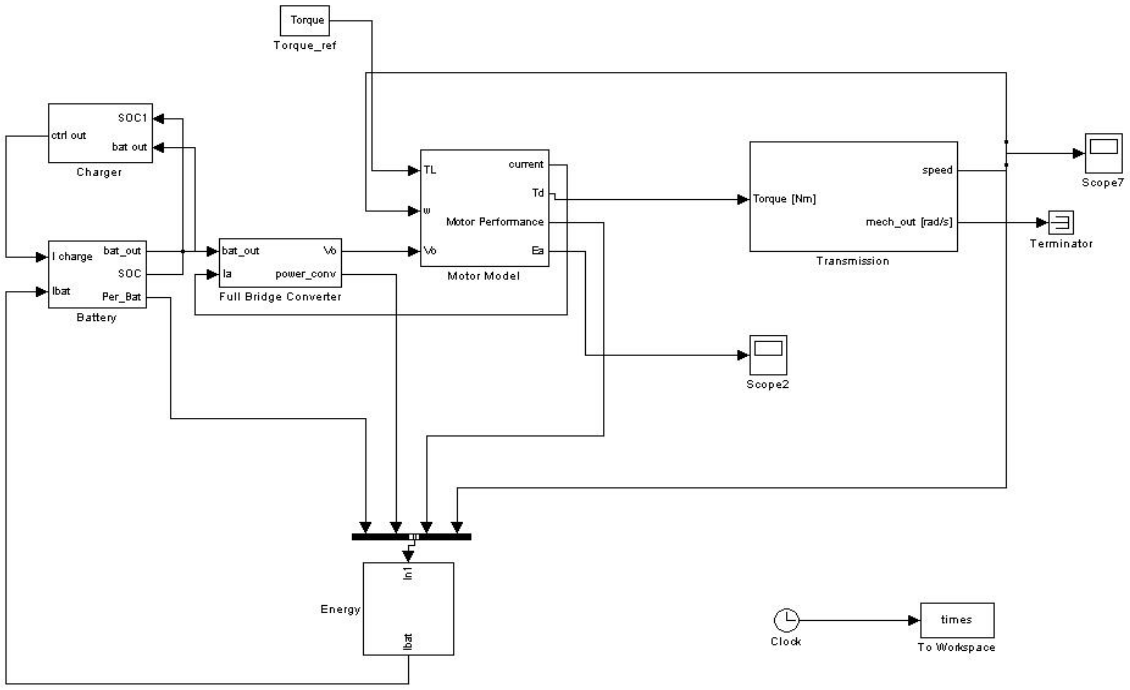

Figure 6.1 Electric traction drive system for electric karting models in Simulink

The algorithm of this electric traction drive system can be seen in the flowchart in Figure 6.2. The reference load was used to calculate stator currents, rotor currents and air gap voltages of the electric motor. The stator and rotor currents were used to detect the normal or regenerative condition because the load torque was assumed to be almost proportional to the stator or rotor currents as described in Section 2.2.1. The stator and rotor currents were used to find the copper losses and the developed power in the electric motor, and the switching and conduction losses in the power electronic converter. The speed of the electric karting was also calculated based on developed torque produced by the electric motor. After the losses in each component were known, the efficiency of each component could also be found. The efficiencies for normal and regenerative conditions were calculated using different formulas for each component as described in Section 2.5.

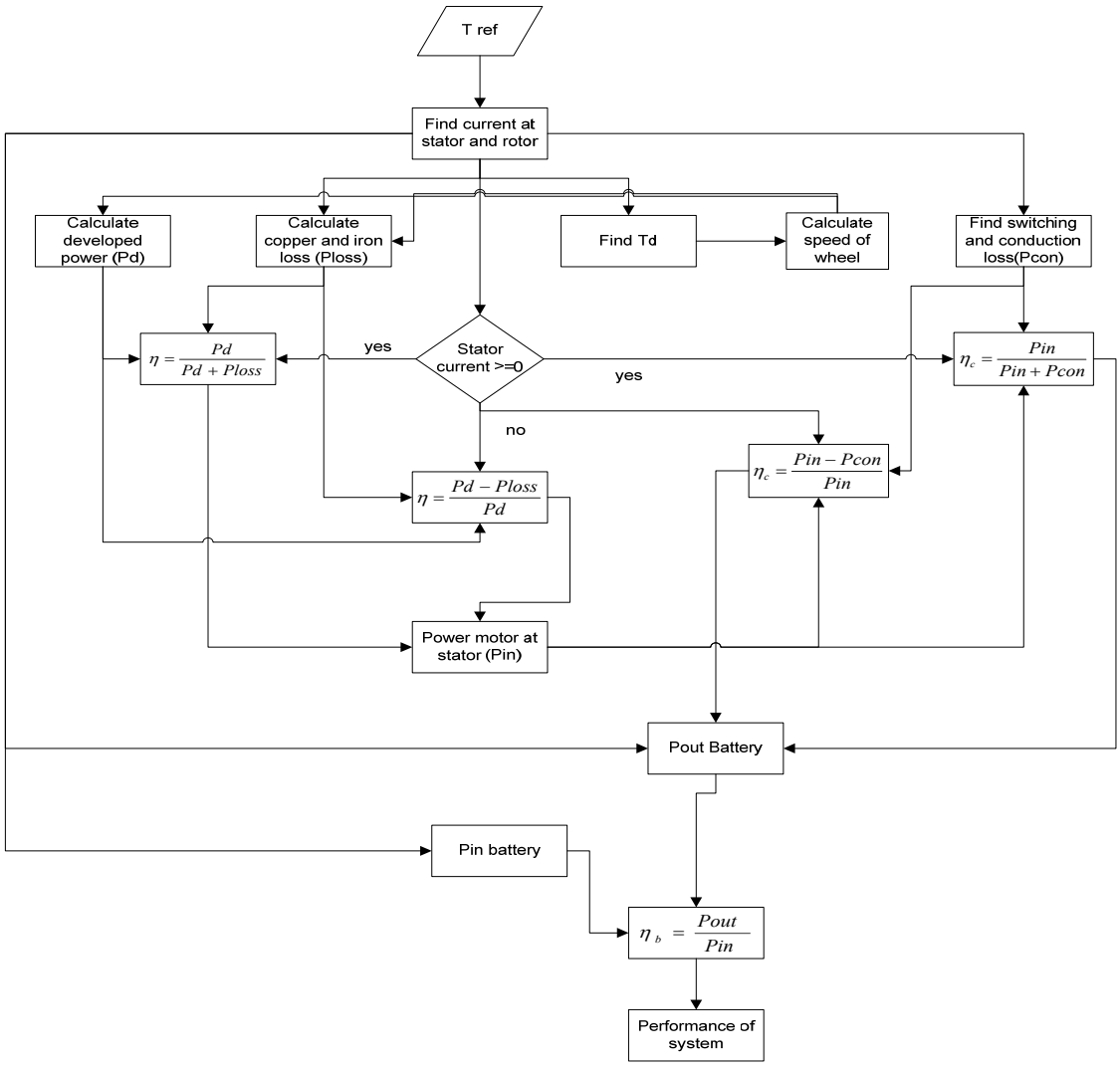

Figure 6.2 Flowchart of the electric traction drive system algorithm.

The input power, output power, and SOC of the battery were also calculated based on the stator currents that were affected by the efficiencies of the electric motor, the power electronic converter and the battery itself. The system's energy use equals the energy output of the battery. Finally, the performance of the complete drive system was calculated and displayed. It includes the SOC of the battery, efficiency of the drive system, and energy usage of the system. The energy from the regenerative braking is limited in the battery.

This simulation ran in 48 seconds and used variable-step ode45 (Dormant-Prince) solver. The relative tolerance was 1e-3. There were also three *m files* that each represents the system parameters, displays the post processing, and includes calculation on the performance of each component of the system.

6.2. Efficiency of the Electric Traction Drive System

According to the data sheet of the electric motor, the rated speed of the motor is 2850 rpm and the rated power is 6000 W. The rated torque of this induction motor was calculated by (2.19) and the result was 20.1 Nm. The speed and torque at the electric karting wheel were between 886 - 1801 rpm and 0 - 47 Nm respectively, as explained in Chapter 3. This speed and torque must be geared to values that have a high efficiency of the electric motor as seen in Figure 5.4. By using (2.7) , the gear ratio

used in this drive system has been selected to 45/21. With this gear ratio, the induction motor operates at speeds between 1889 – 3859 rpm and torques between 0 – 21.9 Nm. The slip of the induction motor was assumed to be constant because the electric motor operates almost in the torque constant region. The mechanical losses of the electric motor and the vehicle dynamic model were assumed to be zero.

The simulation used eight batteries as energy storage with the configuration as shown in Figure 6.3. Therefore, the batteries' capacity was 36 Ah with the equivalent internal resistance of 0.045 Ω and the total weight of 31.2 kg. The output voltage was maintained above the nominal end zone (cut-off) voltage. The result of this simulation can be seen in Figure 6.4 – 6.10.

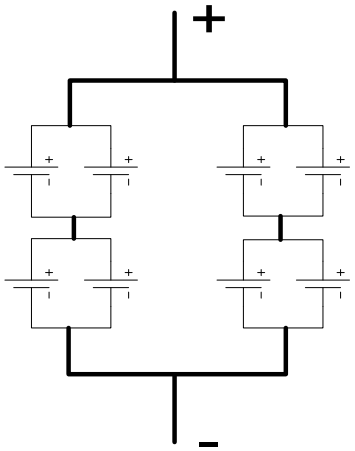

Figure 6.3 Configuration of the batteries.

Calculating from Figure 6.4, the average efficiency of the electric motor was 86.2%. The average efficiencies of the power electronic converter and the battery were 92.7% and 83.5%, respectively. Thus, the total average efficiency of this system was 66.7%. The lower efficiency at the battery occurred as a result of the large current in the equivalent internal resistance of the battery. At regenerative braking condition, the efficiency of the electric drive system was lower than that of normal operation due to the larger current in regenerative braking. Therefore, at regenerative braking condition, the losses increased in the power electronic converter, battery and electric motor. The drop marked with the rectangle in the graph is due to zero crossing in the divide block in Simulink® at regenerative efficiency calculation.

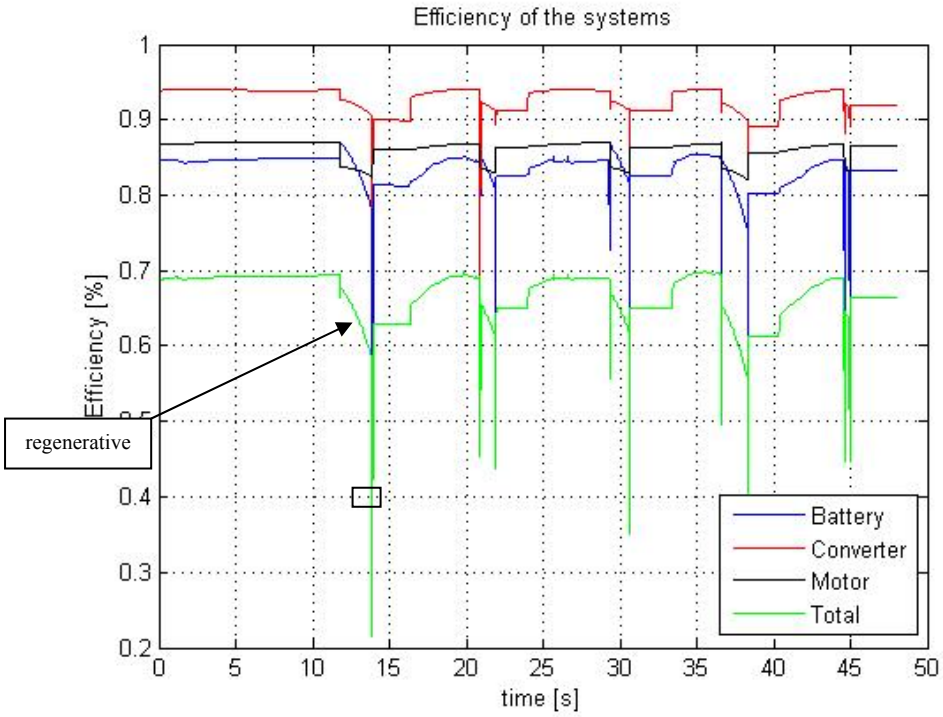

Figure 6.4 Efficiency of the electric traction drive system for electric karting application using the induction motor.

6.3. Power Usage of the Electric Traction Drive System

The average power at the electric motor, power electronic converter, and battery were 5.4 kW, 5.3 kW, and 5.9 kW, respectively, as seen in Figure 6.5. The electric motor output power was higher than the power electronic converter output at regenerative braking condition because the power flow from the induction motor to the power electronic converter is augmented by the large energy from regenerative braking. It is clear that at constant speed, the power usage in the system is constant due to constant torque. This average power for the induction motor is still below the rating of the induction motor.

From Figure 6.5, it is clear that the power at regenerative braking was higher than the power at normal condition. The maximum power of the electric motor at normal condition was 7 kW, but at the regenerative braking, the power of the electric motor reached 13 kW. This large power can affect the reliability and insulation of the electric motor. The large energy could also harm the power electronic converter and battery. The temperature in the components of the power electronics could increase beyond the allowable maximum temperature. This could damage the components of the power electronic converter.

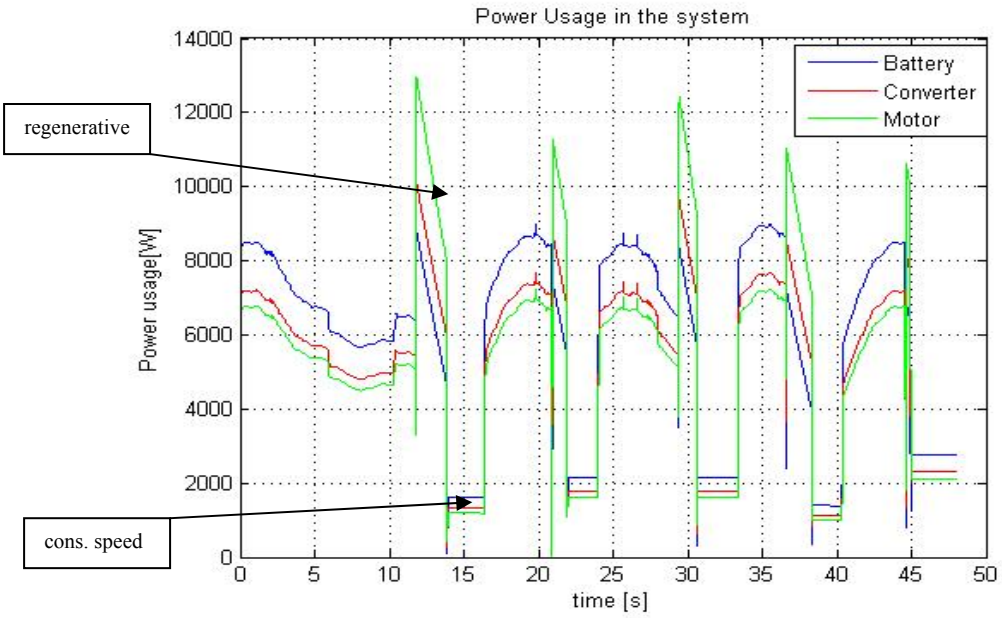

Figure 6.5 Power usage each component of the electric traction drive system for electric karting application using the induction motor.

The energy usage in the electric traction drive system (W_{drive}) for the electric karting can be calculated by integration of the power usage in the drive system (P_{drive}) as shown in (6.1).

$$W_{drive} = \int_0^t P_{drive} dt. \tag{6.1}$$

The total energy used by the drive system is the subtraction of the regenerative energy from the used driving energy and can be seen in Figure 6.6.

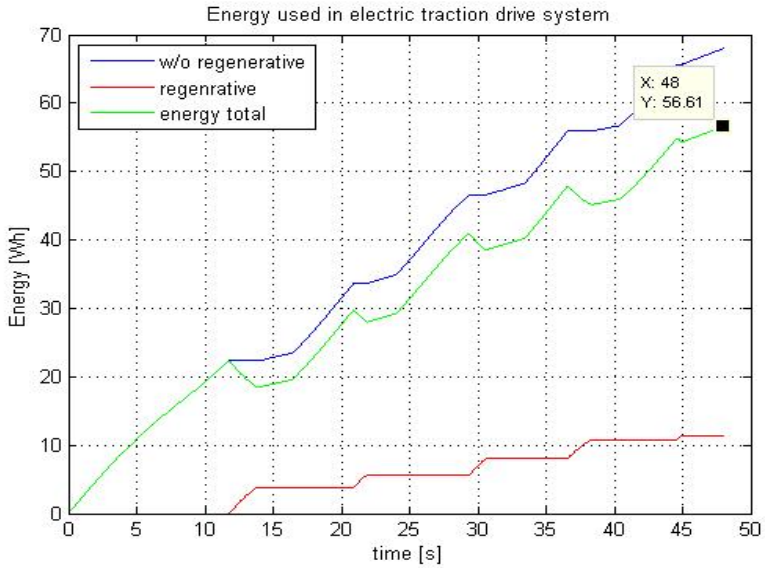

Figure 6.6 Energy used of the electric traction drive system for electric karting application using the induction motor.

Figure 6.6 shows that the regenerative braking supplies a higher energy level in short time compared to normal operation. Consequently, this energy must be considered in designing an electric traction drive system. The total energy for 48 seconds at the electric motor in this drive cycle without regenerative braking was 53.5 Wh. The regenerative braking energy at the electric motor in this drive

cycle was 15 Wh. As a result, the total energy of the electric motor with regenerative braking was 38.5 Wh. The total energy consumed by this electric traction drive system was 67.9 Wh, if the electric traction drive was run without using the regenerative braking energy. The total energy used by the electric traction drive system is 56.6 Wh with the regenerative braking energy supplying the energy (11.4 Wh) to the energy storage that can be seen in Table 6.1.

Table 6.1
Comparison of energy usage

	Regenerative energy [Wh]	W/o regenerative [Wh]		With regenerative [Wh]	
		One lap	13 minutes	One lap	13 minutes
Transmission	18.8	48.7	796.3	30.2	490.8
Electric Motor	15	53.5	869.4	38.5	626.2
Power Elect. Conv.	13.7	57.2	929.4	42	706.1
Battery	11.4	67.9	1104.5	56.6	920

Table 6.1 shows that the total regenerative energy at the battery is lower than the total regenerative braking energy at the electric motor due to losses at the components of the electric drive system.

The energy needed to operate the electric karting for 13 minutes was 920 Wh with regenerative braking, or 1104.5 Wh without regenerative braking. Therefore, the energy available in the battery (48Vdc) must be at minimum 19.2 Ah without regenerative braking, and 23 Ah with regenerative braking.

The average stator current of the electric motor was 75 A, while the maximum current was 150A and the minimum current was -207 A. The negative current means that the electric motor operates as generator. It is clear that the maximum current during regenerative braking is larger than the rated current of the electric motor. Because of the short duration of regenerative braking in the drive cycle, the maximum current for regenerative braking is still acceptable by adding an optional cooler.

6.4. Performance of the Battery

The performance of the battery in the electric traction drive system can be evaluated using the SOC of the battery during the drive cycle. The SOC of the battery can be seen in Figure 6.7. At the end of simulation, the SOC of the battery was 0.9639. If the drive cycle is assumed to be the same for other times, the storage energy can support the electric traction drive system for 22 minutes and 51 seconds. That means the battery can run the electric karting for 13 minutes with that drive cycle.

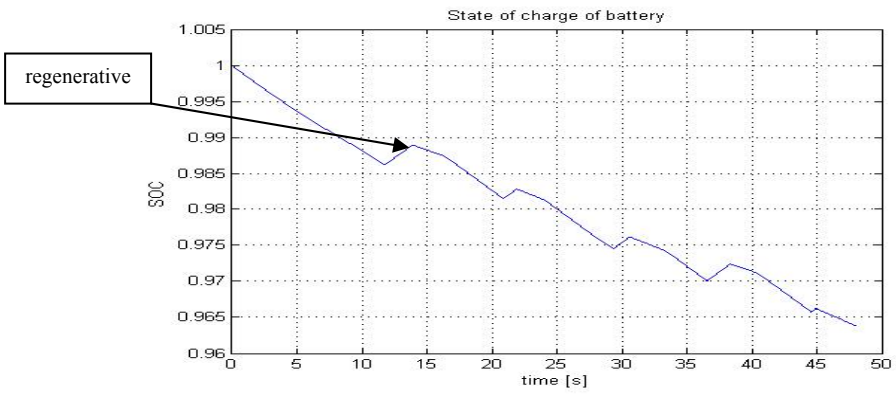

Figure 6.7 State of charge of battery at electric traction drive system for electric karting application using induction motor

The increasing lines represent the charging of the battery from regenerative braking. It is clear that the regenerative braking energy can be used to charge the battery and reduce the energy usage in the system. However, the regenerative braking energy cannot help so much to charge the battery due to the short time of the regenerative braking period and limitation of the battery charging current.

6.5. Performance of the Vehicle Dynamic Model

The speed of the electric karting can be seen in Figure 6.8. It is clear that the maximum speed in this electric karting is 96 km/h.

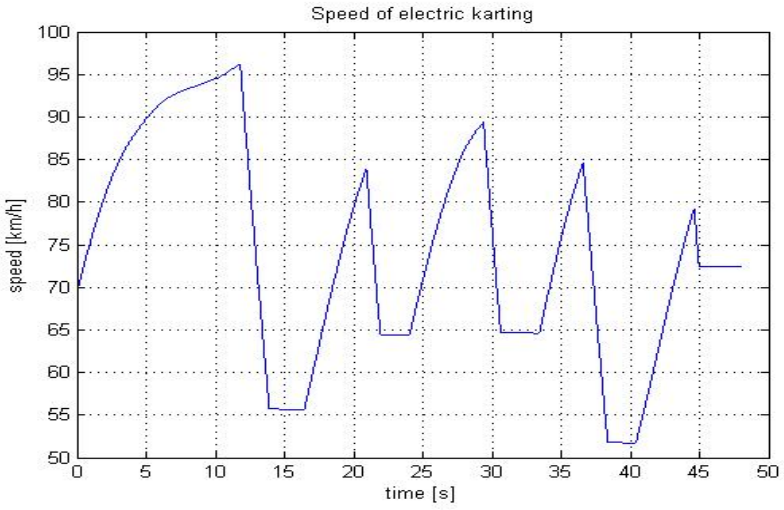

Figure 6.8 Speed of electric karting using the induction motor drive system

A power and torque characteristics as function of the speed can be seen in Figure 6.9. The transmitted power in the electric traction drive cycle increases with the increasing speed due to increasing frequency and voltage until the rated speed. The maximum power occurs in the rated speed. At above the rated speed, the transmitted power decreases again as a result of the decreasing stator and rotor currents. The torque is almost constant at rated torque below the rated speed and will decrease at above the rated speed due to decreasing power transmitted in the electric karting. At regenerative braking condition, the torque is almost constant above the rated torque of the electric motor.

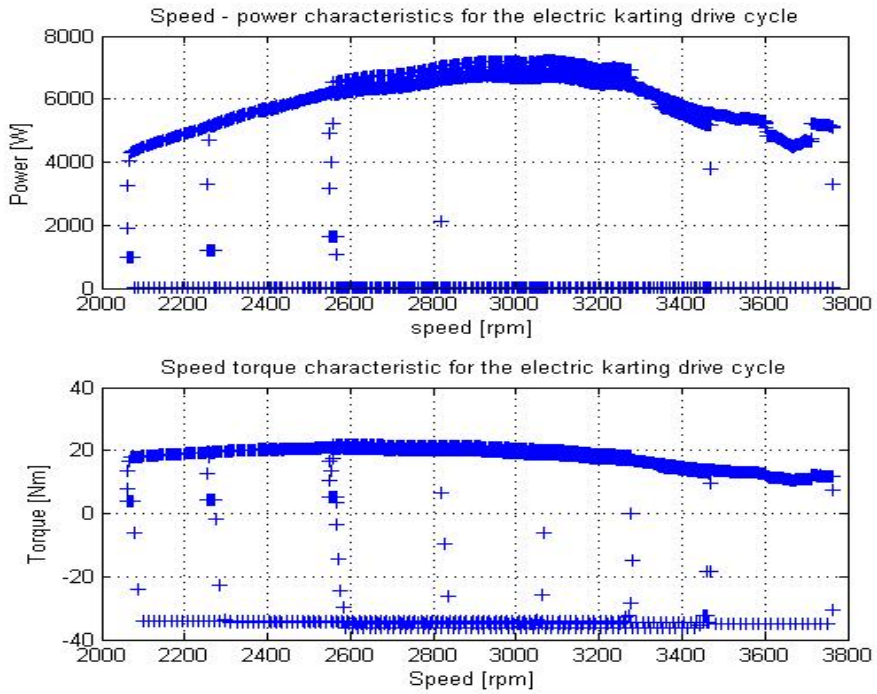

Figure 6.9 Speed – power and torque characteristics of the electric karting using the induction motor drive system

The losses of the battery, power electronic converter and electric motor are almost proportional with the total transmitted power of the electric traction drive system as seen in Figure 6.10.

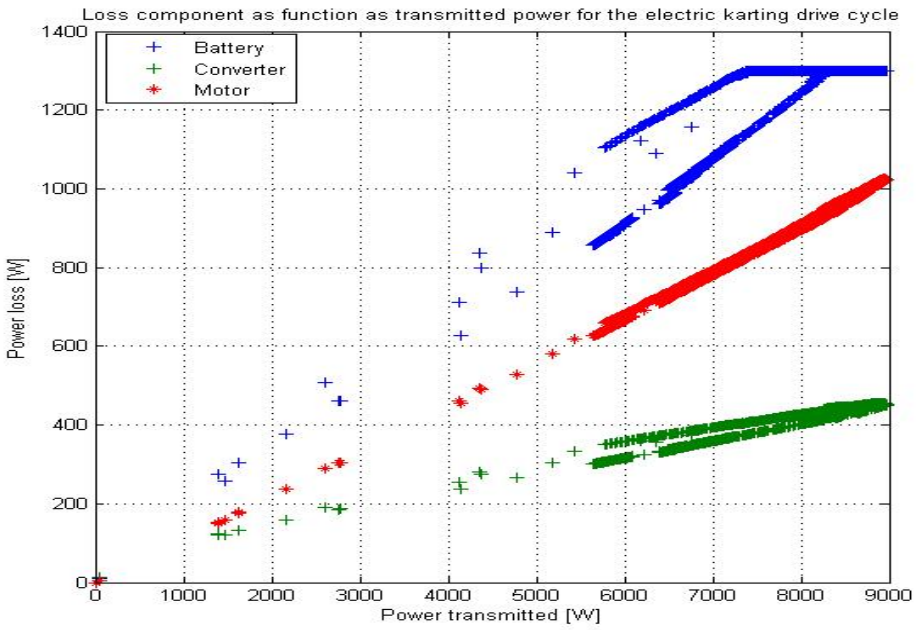

Figure 6.10 Loss components as function as transmitted power for electric karting using induction motor drive system

It shows that the battery losses are the predominant losses in the electric drive system and the power electronic converter losses is the smallest losses in the electric drive system. It is clear that the transmitted power of the drive system is between 5 kW and 9 kW. There are two losses in a

transmitted power due to the regenerative braking effects. The higher loss occurs after the charging the battery from the regenerative braking energy.

6.6. Safety Consideration

The electric karting drive system shall be designed to operate safely in all conditions. The different risks associated with this technology must be carefully assessed. Several international standardization and regulation committees are active on electric vehicle and karting standards, such as IEC TC 69, CENELEC TC 69X, ISO TC22/SC21, CEN TC 301, and CIK-FIA. The different aspects of electric safety that must be considered for electric karting are explained in the following section.

6.6.1. Electric system safety

The aim of the electric system safety is to protect against electric shocks. There are different aspects that must be considered, such as the typical voltage levels that are used in the electric karting. In this thesis, 24-60 Vdc level was used, in compliance with the maximum security levels that are 25 Vac and 60 Vdc at the contact with conductive bodies.

To prevent electrocution through direct or indirect contact, the voltages level must be monitored. The protection of live parts against direct contact can be done by using insulation or inaccessible position. Insulation such as varnish, enamel, coatings are not considered to be insulation as required for protection against direct contact.

The protection against indirect contact is closely related to the protection of frame faults. The unperfected connection between the traction circuit and the karting frame is regarded as a fault. This fault can lead to short circuit, electrocution, and uncontrolled operation. To avoid these faults, a fuse must be installed inside the battery pack. The karting frame shall be isolated from the traction circuit and must not been part of the power electrical circuit. All conductive part shall be connected with an equipotential connection and frame fault leakage detection should be included in routine maintenance.

6.6.2. Functional system safety

The electric karting drive system must ensure a reliable and safe operation of the vehicle. Specific measures should be taken to avoid or prevent unsafe operations such as system activation warning that prevent movement through unintentional actuating of the traction circuit, power-on procedure that avoid possible damage through excessive torque, overcurrent, or fierce acceleration.

The emergency disconnect device must be installed in electric karting. These emergency switches come in at the battery connection or direct-acting emergency buttons. The controller of electric karting must be able to identify the power surge and frame faults.

Some particular safety considerations are to be put forward on regenerative braking so that regenerative braking works through the drive train, on one axle only, and does not work at very low speed or at stand still. The rate of deceleration is limited and not sufficient for an emergency stop. The effect of regenerative braking may be eliminated when the battery is fully charged, so that the battery will not be overcharged. The primary friction brake system should be able to stop the vehicle in all conditions.

6.6.3. Battery safety

The battery is the most critical item in the electric karting because it might entail electrical, mechanical, chemical, and explosion hazards.

In electrical aspect of battery safety, the protection against electrocution by using the conventional enclosures must be considered. Short circuit also must be protected against with the use of fuse links that shall be carefully located to avoid any risk of explosion. Furthermore, the layout of the battery compartment shall be sensibly designed to avoid any unintentional direct contact or short-circuit. The creepage distance between live parts must be observed to minimize leakage currents.

The location of the battery shall be arranged to avoid instability of the electric karting and should be particularly observed when existing ICE karting are converted to electric traction. The battery must be constrained to avoid injury in case of accident.

The nickel-metal hydride (NiMH) battery that is used in the electric karting has a chemical hazard in its electrolyte (potassium hydroxide - sulphuric acid). Precaution should be taken during maintenance. The lead metal in the battery is only released during the disposal and recycling process.

6.6.4. Maintenance, operation, and training

The electric karting must be easy and safe to maintain by the user, in the workshop, and in the manufacturer workshop. The maintenance include battery top-up, routine mechanical maintenance, controller replacement, and major electrical repair. During maintenance, the battery should be disconnected before any intervention is done.

Beside this maintenance, the test of insulation resistance and earth leakage, controller operation, and battery condition is a part of the legal vehicle testing.

7. CONCLUSION AND FUTURE WORK

This chapter presents the summary of the report and suggestions of future work that can be done within this area.

7.1. Summary

In this report, a MATLAB®/SIMULINK® model of an electric traction motor drive system for electric karting was developed. By using the efficiency model for normal and regenerative braking conditions, the models of the induction motor, power electronic converter, and battery were also obtained. In addition, the model of the ideal vehicle dynamics go-kart and charging battery and the basic step to choose the components of the electric traction drive system were presented. The speed profile and torque profile that were used in the simulation were assessed.

The measurements of power, current and voltage of the induction motor for no-load and locked rotor test were performed in the laboratory. The parameters of the induction motor were evaluated by a no-load and a locked rotor test. The mechanical loss of the induction motor was also calculated from the no-load test. The equivalent internal resistance of the battery was also measured in the laboratory by performing a DC load test.

The loss modeling for the induction motor was presented and simulated. It was shown that the highest motor performance occurred at points having a higher speed and lower torque than rated. The power electronic converter loss model was simulated over the load profile. The conduction losses took a significant proportion of the total power electronic converter losses and the MOSFETs consumed more losses compared to the diodes. The conduction losses varied linearly with the square of the load current of the power electronic converter, but the switching loss for the diode was independent of the output power. From the simulation of the battery, the output voltage of the battery will decrease, if the discharge current increase.

Finally, the complete electric traction drive system was simulated and observed. The total average efficiency of the system was 66.7% and the total efficiency depended on the efficiency of the electric motor and the battery that had an efficiency between 86.1% and 83.4%. The power electronic converter components had efficiency higher than 90%. In this simulation, there was no limitation for regenerative braking energy feed into the electric motor. The average power of the entire system and the electric motor were found to be 5.95 kW and 5.4 kW, respectively. The total energy consumed for this electric traction drive system was 56.61 Wh in one lap with the regenerative braking energy and 920 Wh in the whole race. The average stator current in the induction motor was 75 A and this current was below the rated one.

From the case study analysis, the performance of the battery in the electric traction drive system can support the electric traction drive system for 22 minutes and 51 seconds. As a result, this battery can fulfill the requirement that is specified in Section 1.2 where the battery must be capable to support the vehicle for 13 minutes. The type of battery can be changed to other types of battery which have a lower internal resistance but the price will be higher. It is clear that the regenerative braking energy can be used to charge the battery and reduce the energy usage in the system. However, the regenerative braking energy only has a small effect due to the short time of the regenerative braking period.

The proposed electric traction motor drive system has a weight of 52 kg (batteries and electric motor). It does not fulfill the total drive package system weight of the complete drive system.

7.2. Future Works

In this report, the main focus has been placed on the induction motor modeling using the efficiency model on steady state. Thus, there exists much future research scope in improving the behavior of the electric motor, power electronic converter, and battery for dynamics simulation. Furthermore, the use of an advanced traction motor such as the permanent magnet DC motor, permanent magnet synchronous motor, series DC motor, brushless DC motor, and switched reluctance motor, which have even higher efficiencies, might lead to higher system efficiencies.

The regenerative braking energy optimization is also interesting research that can be done. In electric karting, the energy of regenerative braking is very high and short in time.

Another phenomenon to be considered due to the high losses in the electric motor, power electronic converter, and battery is increasing temperature in the electric traction drive system component.

REFERENCES

[1] J. Larminie, J. Lowry, *Electric Vehicle Technology Explained,* John Wiley and Sons, 2003

[2] C. C. Chen, "An overview of electric vehicle technology," *Proceeding of IEEE,* vol. 81, no. 9, pp. 1202-1213, Sept 1993.

[3] M. Ehsani, K. M. Rahman, H. A. Toliyat, "Propulasion system design of electric and hybrid vehicles," IEEE TRANSACTIONS ON INDUSTRIAL ELECTRONICS, VOL. 44, NO. 1, pp. 19-27, FEBRUARY 1997

[4] http://en.wikipedia.org/wiki/Go_karting *last visited 25 February 2009*

[5] http://www.kartelec.com/f/en_actu.htm *last visited 25Februari 2009*

[6] C. Cardoso, J. Ferriera, V. Alves, R. E. Araujo, " The design and implementation of an electric go-kart for education in motor control, " *IEEE International Symposium on Power Electronics, Electrical Drives, Automation, and Motion SPEEDAM 2006,* pp. 1489 – 1494, May 2006.

[7] F. J. Perez-Pinal, C. Nunez, R. Alvarez, M. Gallegos, " Step by step design procedure of an independent-wheeled small EV applying EVLS," *IECON 2006-32nd Annual Conference on IEEE Industrial Electronics,* pp. 1176-1181, Nov 2006.

[8] M. Xianmin, "Propulsion system control and simulation of electric vehicle in MATLAB software environment, "*Proceeding of the 4th World Congress on Intelligent Control and Automation 2002*, pp. 815-818, June 2002.

[9] J. M. Lee, B. H. Co, " Modeling and simulation of electric Vehicle power system, " *Proceeding of the 32nd Intersociety IECEC-97,* vol. 3, pp. 2005-2010, August 1997

[10] S.S. Williamson, A. Emadi, K. Rajashekara, "Comprehensive Efficiency Modeling of Electric Traction Motor Drives for Hybrid Electric Vehicles Propulsion Applications," *IEEE Transaction on Vehicular Technology,* vol. 56, no. 4, pp.1561-1572, July 2007.

[11] Robert Bosch GmbH, *BOSCH-Automotive Handbook*, Robert Bosch GmbH, German, 2002

[12] G. C. D. Sousa, B. K. Bose, " Loss modeling of converter induction machine system for variable speed drive," *Proceeding of the 1992 International Conference on Power electronics and Motion Control,* vol. 1, pp. 114-120, Nov. 1992

[13] J. Soulard, S. Meier, Y. Chin, "Modeling of iron losses in permanent magnet motors with field-weakening capability," *KTH publication of school of electrical engineering,* 2002

[14] Mohamed A. El-Sharkawi, "Fundamentals of Electric Drives," *Brooks/Cole Thomson Learning,* 2000.

[15] J.J. Cathey, "Electric Machines Analysis and Design Applying Matlab®," *McGraw Hill,* 2001

[16] C. Shumei, L. Cheng, S. Liwei," Study on Efficiency Calculation Model of Induction Motors for Electric Vehicles," *IEEE Vehicle Power and Propulsion Conference,* pp. 1-5, Sept 2008

[17] J. Faiz, M. B. B. Sharifian, "Optimal design of an induction motor for an electric vehicle, "Euro*. Trans. Electr. Power 2006*, vol. 16, pp. 15-33, July 2005.

[18] G. Pugsley, C. Chillet, A. Fonseca, A-L. Bui-Van, "New modeling methodology for induction machine efficiency mapping for hybrid vehicles," *IEEE International Electric Machines and Drives Conference 2003*, vol.2, pp. 776-781, June 2003.

[19] S.M. Lukic, A. Emado, " Modeling of Electric Machines for Automotive Applications Using Efficiency Maps," *Electrical Insulation Conference and Electrical Manufacturing & Coil Winding Technology Conference 2003,* pp. 543-550, Sept. 2003.

[20]N. Mohan, T. M. undeland, and W. P. Robbins, ”Power Electronics: Converter, Applications, and Design,” Hoboken, NJ:Wiley, Oct 2002

[21]B.K. Bose, “*Power Electronics and Variable Frequency Drives,”* IEEE Press, New York, 1997.

[22]B.K. Bose, “*Modern Power Electronics and AC Drives,”*Prentice Hall, New York, 2002.

[23] I. Husain, M. S. Islam, “Design, Modeling and Simulation of an Electric Vehicle System, “SAE-*Advanced in Electric Vehicle Technology,* 1999-01-1149, March 1999.

[24]Ali Emadi, “ Handbook of Automotive Power Electronics and Motor Drives,” *CRC Press – Taylor and Francis Groups,* Florida 2005

[25]F. Casanellas ,”Losses in PWM inverter using IGBTs,” *IEE Proc. Electr. Power Appl.,* vol. 141, no. 5, pp. 235-239, September 1994.

[26]P.A. Dahono, Y. Sato, T. Kataoka,” Analysis of conduction losses in inverter,” *IEE Proc. Electr. Power Appl.,* vol. 142, no. 4, pp. 225-232, July 1995

[27]H.L. Chan, D. Sutanto, “A new Battery Model for use with Battery Energy Storage Systems and Electric Vehicle Power Systems,” *IEEE Power Engineering Society Winter Meeting 2000,* vol.1, pp. 470-475, 2000

[28]M. Durr, A. Cruden, S. Gair, J. R. McDonald,” Dynamic Model of a Lead Acid Battery for Use in Domestic Fuel Cell System,” *Journal of Power Source 161*, pp. 1400-1411, 2000

[29]Xiaoling He, “Battery Modeling for HEV Simulation Model development,” *SAE Advanced Hybrid Vehicle Powertrains,* 2001-01-0960, March 2001.

[30]O. Tremblay, L-A. Dessaint. A-I. Dekkiche, “A generic battery model for the dynamic simulation of hybrid electric vehicles, “IEEE *Conference on Vehicles Power and Propulsion VPPC 2007*, pp. 284-289, Sept. 2007.

[31]J. Lee, D. J. Nelson, “Rotating inertia impact on propulsion and regenerative braking for electric motor driven vehicles,” *IEEE conference on Vehicle Power and Propulsion 2005*, pp. 308-314, Sept 2005.

[32]B. Cao, Z. Bai, W. Zhang, “Research on control for regenerative braking of electric vehicle,” *IEEE International Conference on Vehicular Electronics and Safety 2005,* pp. 92-97, Oct 2005.

[33]Z. Junzhi, L. Xin, C. Shanglou, Z. Pengjun, “Coordinated control for regenerative braking system,” *IEEE Vehicle Power and Propulsion Conference (VPPC)*, pp 1-6, Oct. 2008

[34] NEMA Standard MG1

[35]*IEEE Standard test Procedure for Polyphase Induction Motors and generators, Nov 2004*

[36]J. Åström, “Investigation of Issues Related to Electrical Efficiency Improvement of Pump and Fan Drives in Building,” *Licentiate Thesis Electric Power Engineering Chalmers*, June 2008

APPENDIX

This appendix describe about the general term and terminology that is used in the battery.

Battery Basics

· ***Battery Classifications*** – The main area in battery development is between power and energy. So, batteries can be either high-power or high-energy, but not both. Other common classifications are High Durability, meaning that the chemistry has been modified to provide higher battery life at the expense of power and energy.

· ***C- and E- rates*** – C-rate means the discharge current in order to normalize against battery capacity that be used as a measure of the rate at which a battery is discharged relative to its maximum capacity. For example, a 1C rate means that the discharge current will discharge the entire battery in 1 hour. For a battery with a capacity of 100 Amp-hrs, this equates to a discharge current of 100 Amps. A 5C rate for this battery would be 500 Amps, and a C/2 rate would be 50 Amps. Similarly, an E-rate describes the discharge power. A 1E rate is the discharge power to discharge the entire battery in 1 hour.

Battery Condition

Some variables used to describe the present condition of a battery.

· ***State of Charge (SOC)(%)*** – SOC is an expression of the present battery capacity as a percentage of maximum capacity. SOC is generally calculated using current integration to determine the change in battery capacity over time.

.Depth of Discharge (DOD) (%) – The percentage of battery capacity that has been discharged expressed as a percentage of maximum capacity. A discharge to at least 80 % DOD is referred to as a deep discharge.

· ***Terminal Voltage (V)*** – The voltage between the battery terminals with load applied. Terminal voltage varies with SOC and discharge/charge current.

· ***Open-circuit voltage (V)*** – The voltage between the battery terminals with no load applied. The open-circuit voltage depends on the battery state of charge, increasing with state of charge.

· ***Internal Resistance*** – The resistance within the battery, generally different for charging and discharging, also dependent on the battery state of charge. As internal resistance increases, the battery efficiency decreases and thermal stability is reduced as more of the charging energy is converted into heat.

Battery Technical Specifications

· ***Nominal Voltage (V)*** – The reference voltage of the battery.

· ***Cut-off Voltage*** – The minimum allowable voltage.

· ***Capacity or Nominal Capacity (Ah for a specific C-rate)*** – The total Amp-hours available when the battery is discharged at a certain discharge current (specified as a C-rate) from 100 percent state-of-charge to the cut-off voltage.

· ***Energy or Nominal Energy (Wh (for a specific C-rate))*** – The total Watt-hours available when the battery is discharged at a certain discharge current (specified as a C-rate) from 100 percent state-of-charge to the cut-off voltage.

· ***Cycle Life (number for a specific DOD)*** – The number of discharge-charge cycles the battery can experience before it fails to meet specific performance criteria. Cycle life is estimated for specific charge and discharge conditions. If battery has higher the DOD, the cycle of life is lower.

· ***Specific Energy (Wh/kg)*** – The nominal battery energy per unit mass. Specific energy is a characteristic of the battery chemistry and packaging. It determines the battery weight required to achieve a given electric range

Specific Power (W/kg) – The maximum available power per unit mass. It determines the battery weight required to achieve a given performance target.

· ***Energy Density (Wh/L)*** – The nominal battery energy per unit volume. It determines the battery size required to achieve a given electric range.

· ***Power Density (W/L)*** – The maximum available power per unit volume. It determines the battery size required to achieve a given performance target.

· ***Maximum Continuous Discharge Current*** – The maximum current at which the battery can be discharged continuously.

· ***Maximum 30-sec Discharge Pulse Current*** –The maximum current at which the battery can be discharged for pulses of up to 30 seconds.

· ***Charge Voltage*** – The voltage that the battery is charged to when charged to full capacity.
· ***Float Voltage*** – The voltage at which the battery is maintained after being charge to 100 percent SOC to maintain that capacity by compensating for self-discharge of the battery